The Journal of Physiology

Acute introduction of monomeric or multimeric α-synuclein induces distinct impacts on synaptic vesicle trafficking at lamprey giant synapses

Cristina Román-Vendrell[1], Jaqulin N. Wallace[1], Aurelia Hays Watson[2], Meral Celikag[2], Tim Bartels[2] and Jennifer R. Morgan[1]

[1] *The Eugene Bell Center for Regenerative Biology and Tissue Engineering, Marine Biological Laboratory, Woods Hole, Massachusetts, USA*
[2] *UK Dementia Research Institute, University College London, London, UK*

Handling Editors: Katalin Toth & Samuel Young

The peer review history is available in the Supporting Information section of this article (https://doi.org/10.1113/JP286281#support-information-section).

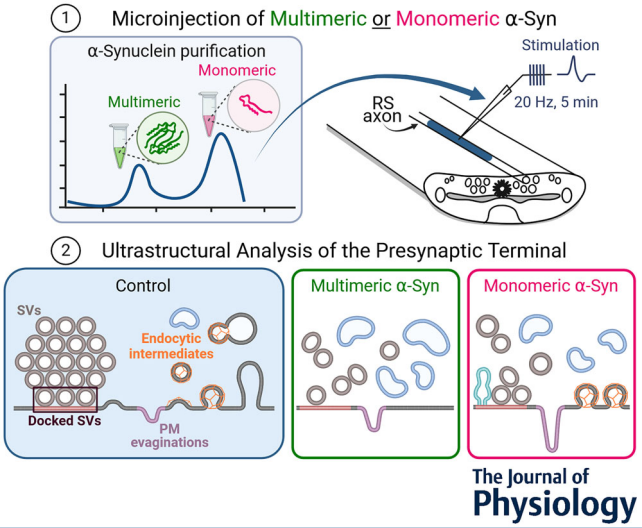

Abstract figure legend Monomeric and multimeric α-synuclein were purified from HEK cells and delivered to lamprey reticulospinal (RS) synapses via axonal microinjection, followed by stimulation (20 Hz, 5 min). Ultrastructural analysis showed that both α-synuclein species impaired intracellular vesicle trafficking, leading to synaptic vesicle loss and endosome buildup. While multimeric α-synuclein reduced synaptic vesicle docking, monomeric α-synuclein induced a greater expansion of the plasma membrane (PM), inhibited clathrin-mediated endocytosis and caused atypical fusion at the active zone. This highlights the distinct effects of monomeric and multimeric α-synuclein on synaptic function. Created with BioRender.com.

Cristina Roman-Vendrell earned her Ph.D. in Physiology from the University of Puerto Rico School of Medicine under the supervision of Dr Guillermo Yudowski and Dr Jorge Miranda. She is currently a Postdoctoral Fellow in Dr. Jennifer Morgan's lab at the Marine Biological Laboratory (MBL). Her research focuses on understanding the molecular mechanisms underlying synaptic function and dysfunction, particularly in the context of Parkinson's disease. Cristina is now studying presynaptic endosomal trafficking and the mechanisms underlying synaptic deficits in neurodegenerative diseases.

DOI: 10.1113/JP286281

Abstract Synaptic aggregation of α-synuclein often occurs in Parkinson's disease (PD), dementia with Lewy bodies (DLB) and other synucleinopathies and is associated with cognitive deficits and dementia. Thus, it is important to understand how accumulation of α-synuclein affects synapse structure and function. Native, physiological α-synuclein comprises a mixture of tetramers and related physiological oligomers (60–100 kDa) in equilibrium with monomeric α-synuclein. We previously demonstrated that acutely increasing the levels of physiological α-synuclein impaired intracellular synaptic vesicle trafficking and produced a pleiotropic phenotype, raising questions about which aspects of the synaptic phenotype were due to multimeric versus monomeric α-synuclein. Here, we address this by taking advantage of the unique features of the lamprey giant reticulospinal (RS) synapse, a vertebrate synapse that is amenable to acute perturbations of presynaptic processes via microinjection of purified proteins. α-Synuclein monomers and multimers were purified from HEK cells and separately introduced to lamprey synapses. Ultrastructural analysis revealed that both multimeric and monomeric α-synuclein impaired intracellular vesicle trafficking, leading to a loss of synaptic vesicles and buildup of endosomes. However, while monomeric α-synuclein additionally induced atypical fusion/fission at the active zone and impaired clathrin-mediated endocytosis, multimeric α-synuclein did not. Conversely, multimeric α-synuclein led to a decrease in synaptic vesicle docking, which was not observed with monomeric α-synuclein. These data provide further evidence that different molecular species of α-synuclein produce distinct and complex impacts on synaptic vesicle trafficking and reveal important insights into the cell biological processes that are affected in PD and DLB.

(Received 7 June 2024; accepted after revision 22 October 2024; first published online 11 November 2024)
Corresponding author J. R. Morgan: The Eugene Bell Center for Regenerative Biology and Tissue Engineering, Marine Biological Laboratory, 7 MBL St., Woods Hole, MA 02543, USA. Email: jmorgan@mbl.edu

Key points

- α-Synuclein accumulation at synapses is associated with cognitive decline and dementia in Parkinson's disease and other synucleinopathies.
- We previously showed that acute introduction of excess human brain-derived α-synuclein to lamprey giant synapses caused pleiotropic phenotypes on synaptic vesicle trafficking, probably due to the mixture of molecular species of α-synuclein.
- Here, we dissected which aspects of the synaptic phenotypes were caused by monomeric (14 kDa) or multimeric (60–100 kDa) α-synuclein by purifying each molecular species and introducing each one separately to synapses via axonal microinjection.
- While monomeric α-synuclein inhibited clathrin-mediated synaptic vesicle endocytosis, multimeric α-synuclein primarily impaired endosomal trafficking.
- These findings reveal that different molecular species of α-synuclein have distinct impacts on synapses, suggesting different cellular and molecular targets.

Introduction

α-Synuclein is a presynaptic protein that regulates exocytosis and endocytosis and is therefore critical for maintaining proper neurotransmission (Bendor et al., 2013; Greten-Harrison et al., 2010; Logan et al., 2017; Schechter et al., 2020; Sharma & Burre, 2023; Vargas et al., 2014). In Parkinson's disease (PD), dementia with Lewy bodies (DLB) and other synucleinopathies, α-synuclein accumulates and aggregates abnormally throughout neurons and neurites, including at presynapses (Kramer & Schulz-Schaeffer, 2007; Schulz-Schaeffer, 2010; Spillantini et al., 1998; Spinelli et al., 2014). Synaptic aggregation of α-synuclein is associated with cognitive disorders and dementia in these diseases and likely represents an early stage in the pathophysiology states (Schulz-Schaeffer, 2010; Sharma & Burre, 2023; Sulzer & Edwards, 2019). Thus, determining the precise impacts of excess α-synuclein at synapses is crucial for understanding the cellular and physiological mechanisms

that lead to synaptic pathologies in several common neurodegenerative diseases.

Initial studies performed in mammalian neurons revealed that overexpression of α-synuclein severely impaired local synaptic vesicle trafficking at presynapses, specifically exocytosis/endocytosis dynamics as well as vesicle re-clustering after endocytosis (Nemani et al., 2010; Scott & Roy, 2012; Scott et al., 2010). However, α-synuclein overexpression also induced compensatory downregulation of several key presynaptic proteins, including synapsin, amphiphysin, VAMP2 and complexin (Bridi & Hirth, 2018; Nemani et al., 2010; Scott et al., 2010). While α-synuclein overexpression is a good model for the disease states, the compensatory change in other presynaptic proteins also makes it challenging to determine the direct and specific impacts of excess α-synuclein on synapses. To address this question, we and others have turned toward acute perturbation strategies, where α-synuclein levels can be manipulated over shorter time scales, circumventing the molecular compensation that often occurs with chronic overexpression. Giant synapse models, such as the lamprey giant reticulospinal (RS) synapse and the mammalian calyx of Held, have proven particularly useful for these types of investigations because the α-synuclein protein can be microinjected or dialysed directly into the presynapse. Using lamprey giant RS synapses, we began by acutely increasing the levels of α-synuclein two to three times the estimates for endogenous α-synuclein, which is in line with overexpression levels observed in familial PD and DLB cases (Kramer & Schulz-Schaeffer, 2007; Miller et al., 2004; Singleton et al., 2003). When we introduced excess recombinant human α-synuclein (monomeric) to lamprey synapses, there was a rapid and robust inhibition of clathrin-mediated synaptic vesicle endocytosis and bulk endocytosis, which led to a severe depletion of synaptic vesicles and remarkably slower exocytosis–endocytosis kinetics (Banks et al., 2020; Busch et al., 2014; Wallace et al., 2024). The inhibition of endocytosis by α-synuclein was subsequently corroborated at the mammalian calyx of Held, where elegant capacitance measurements have additionally shown that acutely increasing α-synuclein had little effect on exocytosis (Eguchi et al., 2017; Xu et al., 2016). Thus, accumulation of α-synuclein primarily inhibits synaptic vesicle endocytosis at vertebrate synapses.

Under normal physiological conditions, α-synuclein comprises multiple molecular species in neurons, raising questions about their overlapping or distinct functions and impacts at synapses. Physiological α-synuclein exists as tetramers and related oligomers (60–100 kDa), which we call 'multimers', in equilibrium with α-synuclein monomers (14–17 kDa) and dimers (34 kDa) (Bartels et al., 2011; Burre et al., 2014; Chandra et al., 2003; Gurry et al., 2013; Roman-Vendrell et al., 2021). Altering the normal equilibrium of these molecular species of α-synuclein leads to neurotoxicity. Specifically, point mutations that destabilize α-synuclein multimers increased the content of monomeric α-synuclein and led to increased α-synuclein aggregation and neurotoxicity in cell lines and PD animal models (Dettmer, Newman, Soldner et al., 2015; Nuber et al., 2018). These results are in line with the aforementioned acute perturbation studies, where introduction of monomeric human α-synuclein led to severe disruptions of vesicle endocytosis at lamprey and mammalian synapses and therefore synaptic toxicity. Similarly, acute introduction of α-synuclein dimers to lamprey synapses also inhibited vesicle endocytosis, but at a slightly earlier stage. Whereas monomeric α-synuclein inhibited the uncoating of clathrin-coated vesicles (CCVs), dimeric α-synuclein inhibited fission of clathrin-coated pits (CCPs) from the plasma membrane (Banks et al., 2020; Medeiros et al., 2017). Moreover, native physiological α-synuclein isolated from the brains of neuropathologically normal human subjects moderately impaired intracellular vesicle trafficking, as evidenced by a buildup of endosomal vesicles, without affecting clathrin-mediated endocytosis (CME) from the plasma membrane (Roman-Vendrell et al., 2021). Physiological α-synuclein also induced atypical fusion/fission events at the active zone, which were previously unseen (Roman-Vendrell et al., 2021). Thus, we concluded from these studies that different molecular species of α-synuclein caused distinct impacts on synaptic vesicle trafficking (Medeiros et al., 2018). However, because the physiological, brain-derived α-synuclein comprised a mixture of multimers and monomers, it was difficult to ascertain which aspects of the synaptic phenotype were caused by each molecular species, prompting the current study.

Here, we isolated and purified multimeric and monomeric human α-synuclein from mammalian HEK cells and introduced them individually to lamprey giant synapses. We now demonstrate that multimeric α-synuclein isolated from mammalian HEK cells impaired intracellular vesicle trafficking at presynapses, largely recapitulating the phenotypes caused by physiological brain-derived human α-synuclein. Purified monomeric α-synuclein additionally impaired CME and induced atypical fusion/fission events at the plasma membrane. These findings provide additional evidence that, when in excess, different molecular species of α-synuclein produce distinct impacts on synaptic vesicle trafficking, implicating a complex physiological response during early synaptic pathologies that occur in PD and DLB.

Methods

Ethical approval

All animal procedures were conducted at the Marine Biological Laboratory (MBL) in Woods Hole, Massachusetts, USA, as approved by the Institutional Animal Care and Use Committee at the Marine Biological Laboratory and in accordance with laws, regulations, guidelines and policies established by the National Institutes of Health and Public Health Service (PHS) Policy on Humane Care and Use of Laboratory Animals. All research at the MBL involving use of vertebrate animals is covered under the OLAW/PHS Assurance no.: D16-00039 (A3070-01). All authors have reviewed the ethical principles under which *The Journal of Physiology* operates and confirm that their work complies with the animal ethics checklist provided.

Animals

Late-stage larval sea lampreys (*Petromyzon marinus*, RRID:NCBITaxon_7757), ∼5–7 years old (11–13 cm), males and females, were used for these studies, although they are sexually undifferentiated at this stage of their life cycle (Ajmani et al., 2021). All lampreys were wild caught by either Acme Lamprey Company (Harrison, ME, USA) or Lamprey Services, Inc. (Luddington, MI, USA) and housed in the laboratory for several months at room temperature (RT) in circulating, oxygenated fresh water along with a sand substrate originating from their home streams. At this stage in their life cycle, larval lampreys are gill feeders and do not require an additional feeding regime. For all experiments, lampreys were anaesthetized in 0.2 g/l tricaine methanesulfonate (Syncaine, MS-222; Syndel, Ferndale, WA, USA) diluted in lamprey tank water. Anaesthesia was deemed complete by a loss of swimming behaviour and muscle tone, slowed gill movements, and lack of response to a tail pinch. After anaesthesia, lampreys were euthanized by rapid decapitation and pithing, and terminal tissue harvest of spinal cords was performed for further experimentation. No survival surgeries were performed in this study.

Protein purification

HEK-derived monomeric and multimeric α-synuclein. Lysates from HEK293 transiently overexpressing α-synuclein C-term Strep II-tagged were purchased from GeneScript (Piscataway, NJ, USA) and purified following the method described by de Boni et al. (2022). In summary, α-synuclein from the HEK293 α-synuclein C-term Strep II-tagged lysates was immunoprecipitated using StrepTrap 5 ml columns (GE Healthcare, Hatfield, UK). The procedure involved lysing the cells, ultracentrifuging them at 100,000 *g* for 1 h at 4°C, and measuring the protein content in the supernatant. The lysate was then cross-linked and loaded onto pre-equilibrated Strep Tag 5 ml columns. Unbound samples were washed out with PBS buffer (pH 7.4), and the bound sample was eluted using an elution buffer containing 2.5 mM desthiobiotin (Merck Life Sciences, Dorset, UK) in PBS (pH 7.4). Peak fractions of monomeric or multimeric α-synuclein were pooled and further purified via gel filtration on a HiPrep Sephacryl S-200HR 16/60 gel filtration column (GE Healthcare, Hatfield, UK) using 50 mM NH 4Ac (pH 7.4) as running buffer. Peak fractions (>95% pure, by Coomassie Brilliant Blue-stained SDS-PAGE) were pooled, aliquoted, lyophilized and stored at −80°C. For mock controls, HEK cells without the αS tag underwent the same affinity purification process. The mock controls, containing only potential contaminants of the affinity step, were further used for determination of purity via LC-MS/MS and background subtraction in circular dichroism (CD) spectroscopy as in de Boni et al. (2022).

***Escherichia coli*-derived monomeric α-synuclein.** BL21(DE3) *E. coli* (New England Biolabs, Ipswich, MA, USA) were transformed with the pET21a-based constructs, and single colonies were inoculated in LB-ampicillin. Cultures were induced at an OD 600 of 0.5 with 1 mM isopropyl 1-thio-beta-D-galactopyranoside (IPTG) (Merck Life Sciences, Dorset UK) for 4 h. After harvesting, the cell pellet was resuspended in 20 mM Tris buffer and 25 mM NaCl (pH 8) and lysed by boiling for 15 min. The supernatant from a 20 min, 20,000 *g* spin of the lysate was then processed further. The sample was loaded on two 5 ml (tandem) HiTrap Q HP anion exchange columns (GE Healthcare, Hatfield, UK) equilibrated with 20 mM Tris buffer and 25 mM NaCl (pH 8). α-Synuclein was eluted from the columns with a 25–1000 mM NaCl gradient of 20 mM Tris buffer and 1 M NaCl (pH 8). Peak fractions were pooled and further purified via gel filtration on a HiPrep Sephacryl S-200HR 16/60 gel filtration column (GE Healthcare, Hatfield, UK) using 50 mM NH 4Ac (pH 7.4) as running buffer. Peak fractions (>95% pure, by Coomassie Brilliant Blue-stained SDS-PAGE, Fisher Scientific, Loughborough, UK) were pooled, aliquoted, lyophilized and stored at -20°C.

CD spectroscopy

α-Synuclein samples were added to a 1 mm path length quartz cuvette for far-UV CD spectroscopy and analysed using a J-1500 CD spectrometer (Jasco, Heckmondwike, UK) at 25°C. Temperature control with an accuracy of 0.1°C was achieved with a

heating/cooling accessory equipped with a Peltier element (PFD-425S) connected to a water thermostatic bath. Buffer spectra were recorded and subtracted. The helicity of the protein (i.e. the percentage of the entire protein sequence in an α-helical state) was obtained from the mean residue ellipticities, Θ_{222}, according to $f_{helix} = (\Theta_{222} - \Theta_{coil})/(\Theta_{coil} - \Theta_{helix})$ where %helicity = 100 f_{helix}. Here the mean residue ellipticities at 222 nm for the completely unfolded and completely folded peptides were obtained from $\Theta_{coil} = 640 - 45$ T/°C and $\Theta_{helix} = 40{,}000(1\text{-}2.5/n)+100$T/°C, where n is the number of amino acids in the polypeptide.

Western blotting

Protein samples were rehydrated in lamprey internal solution (180 mM KCl, 10 mM HEPES-K^+, pH 7.4). Next, 250 ng each of α-synuclein from HEK 293 cells (monomers, multimers) was run on a 12% SDS-PAGE gel alongside recombinant wild-type (WT) human α-synuclein, purified from *E. coli* (rPeptide; Watkinsville, GA, USA), and α-synuclein phosphorylated at serine 129 (pS129) (Proteos, Kalamazoo, MI, USA). Following overnight transfer to nitrocellulose membrane, western blots were performed using standard procedures. Briefly, the membranes were blocked in 5% milk in TBST with 0.1% Tween-20 for 30 min at RT. Membranes were then incubated for 2 h at RT in primary antibody: rabbit monoclonal anti-α-synuclein antibody (1:1000; [MJFR1] ab138501; Abcam, Cambridge, MA, USA; RRID:AB_2537217) or a rabbit monoclonal anti-pS129 α-synuclein antibody (1:1000; [D1R1R]; Cell Signaling, Inc., Danvers, MA, USA; RRID:AB_2798868) diluted in TBST. After washing, membranes were incubated for 1 h at RT in HRP-conjugated goat anti-rabbit IgG (H+L) secondary antibody (1:1000; Thermo Fisher Scientific, Waltham, MA, USA). Protein bands were detected by enhanced chemiluminescence (Pierce ECL Western blotting substrate; Thermo Fisher Scientific), and blots were imaged on an Azure Imaging System 300 (Azure Biosystems, Dublin, CA, USA).

Microinjection and stimulation

For the injection experiments, segments of lamprey spinal cords (2–3 cm in length) were dissected and pinned ventral side up in a Sylgard-lined dish containing fresh, oxygenated Lamprey Ringer solution (100 mM NaCl, 2.1 mM KCl, 1.8 mM $MgCl_2$, 4 mM glucose, 2 mM HEPES, 0.5 mM L-glutamine, 2.6 mM $CaCl_2$, pH 7.4). Axonal microinjections were performed as previously described (Walsh et al., 2018). We started with 50 µg each of lyophilized HEK-derived monomeric and multimeric α-synuclein and resuspended both samples in equivolumes of lamprey internal solution (180 mM KCl, 10 mM HEPES K^+, pH 7.4). Due to the different molecular weights, this resulted in a final pipette concentration of ∼115 µM for monomeric α-synuclein and ∼20 µM for multimeric α-synuclein. Samples were then loaded into glass microelectrodes with a resistance of 20–25 MΩ for injection into giant RS axons. Microinjections were performed using small pulses of N_2 (5–10 ms, 40 psi, 0.2 Hz) delivered via a Toohey Spritzer. Co-injection with a fluorescent dye approximating the molecular weights of multimeric and monomeric α-synuclein [Invitrogen, fluorescein dextran, 10,000 MW or 70,00 MW, lysine fixable (Fluoro-Emerald); Thermo Fisher Scientific, Waltham, MA, USA] allowed us to determine the spread of the protein along the axon with respect to the injection site. After injection, α-synuclein samples were typically diluted ∼10–20 times near the injection site and up to 200 times farther away. The giant RS axons were then stimulated using current injections (30–100 nA, 1 ms) at 20 Hz for 5 min to evoke action potentials, which induced synaptic vesicle exocytosis/endocytosis.

Immunofluorescence imaging

As a proxy to confirm successful α-synuclein injections, some lamprey spinal cords were fixed in 4% paraformaldehyde (Electron Microscopy Sciences, Hatfield, PA, USA), 0.1 M PBS pH 7.4, followed by imaging of the co-injected fluorescein dextran. In other experiments, to confirm synaptic localization of injected α-synuclein, we also performed whole mount immunofluorescence on lamprey spinal cords after axonal injection of *E. coli*-derived recombinant human α-synuclein. The injected α-synuclein was detected using a human-specific α-synuclein antibody (MJFR1, 1:100) that does not recognize endogenous lamprey synuclein (Wallace et al., 2024). Synaptic vesicles were labelled with a mouse monoclonal antibody against SV2 (1:100), deposited to the Developmental Studies Hybridoma Bank by K. M. Buckley (DSHB Cat. no. SV2, RRID:AB_2315387). The secondary antibodies used were AlexaFluor Plus 488 goat anti-rabbit IgG and AlexaFluor Plus 594 or 647 goat anti-mouse IgG [H+L; Invitrogen] (Thermo Fisher Scientific, Waltham, MA, USA).

Axonal images of the co-injected fluorescein dextran were acquired using an HC PL APO 20× objective (0.75 NA, 1× optical zoom) on a Leica DMi8 inverted microscope. Following immunofluorescence, the giant axons of interest were initially identified by the AlexaFluor 488 signals associated with the injected α-synuclein protein. Further images of the axons and their synapses were acquired using a 10× Plan-Apochromat (0.45 NA, 1× optical zoom) objective and a 40× Plan-Apochromat (1.4

NA, 2× optical zoom) on a Zeiss LSM780 AxioObserver microscope, respectively.

Electron microscopy and image analysis

For electron microscopy experiments, the lamprey spinal cords with α-synuclein-injected axons were fixed immediately at the end of the stimulation period in 3% glutaraldehyde, 2% paraformaldehyde in 0.1 M sodium cacodylate buffer pH 7.4 (Electron Microscopy Sciences, Hatfield, PA, USA), for >3 h at RT followed by overnight at 4°C. Subsequently, fixed spinal cords were processed for electron microscopy as described in Walsh et al. (2018), embedded in Embed-812 resin, ultrathin sectioned to 70 nm, and placed on copper Formvar slot grids (Electron Microscopy Sciences, Hatfield, PA, USA). Sections were counterstained with 2% uranyl acetate and 0.4% lead citrate. Synapses within the injected axons were imaged at 37,000× or 59,000× magnification using a JEOL JEM - 200CX transmission electron microscope (JEOL, Peabody, MA, USA) using a Hamamatsu C8484-05G Digital CCD side mount camera (Hamamatsu Photonics, Shizuoka, Japan). Synapse images were analysed across three defined ranges of distances relative to the injection site, which broadly represent: High concentration (30–140 μm), Low concentration (145–390 μm) and Control (>400 μm), where no protein had diffused. Based on the diffusion of the co-injected fluorescent dye, we estimate that monomeric α-synuclein was diluted to a final axonal concentration ranging from ∼1–5 μM (Low concentration) to ∼6–12 μM (High concentration). Multimeric α-synuclein was diluted a final axonal concentration ranging from ∼0.1–0.9 μM (Low concentration) to ∼1–2 μM (High concentration).

Morphometric analyses were conducted on $n = 26$–39 synapses derived from $N = 2$–3 axons(2–3 animals) per experimental condition. The researcher who performed these analyses was blinded to the experimental conditions. Measurements of synaptic membranes from a single section obtained at or near the centre of the active zone were quantified in Fiji (ImageJ), as previously described (Busch et al., 2014; Roman-Vendrell et al., 2021; Soll et al., 2020; Walsh et al., 2018). These included the number, size and eccentricity of synaptic vesicles (SVs), plasma membrane (PM) evaginations, cisternae (cist), and clathrin-coated pits and vesicles (CCP/Vs). CCP/Vs stages (1–4) were defined as follows: Stage 1, initiation of CCP formation; Stage 2, maturation of CCP; Stage 3, vesicle fission; Stage 4, free CCVs. PM evaginations were measured as the curved line distances between each edge of the active zone (right and left) and a point at 1 μm straight line distance along the inner axolemma, and then averaged. Vesicles >100 nm in diameter were counted as cisternae, which are presumptive endosomes. These measurements were used to perform a total membrane analysis, as previously described (Banks et al., 2020; Medeiros et al., 2017; Roman-Vendrell et al., 2021; Wallace et al., 2024). Additionally, we analysed the number of 'fusosomes', defined as atypical vesicles that were contiguous with the active zone and therefore appeared to be fusing with the plasma membrane (Roman-Vendrell et al., 2021). Three-dimensional reconstructions of synapses generated from five serial electron micrographs were generated using Reconstruct software 1.1.0.0 (Fiala, 2005). SV distribution and nearest-neighbour analyses were performed as in Wallace et al. (2024). Briefly, to obtain the SV distribution at synapses, the active zone was traced and used as a reference line to determine the shortest distance between it and the centre position of each SV within a 1000 nm radius. Any SV located up to 50 nm from the active zone trace was marked as a docked SV. From these data, the nearest-neighbour distances were also calculated using the centre positions of each SV. SV distribution and nearest-neighbour data were acquired using MATLAB 9.13.0 (The MathWorks, Natick, MA, USA; R2022b; RRID:SCR_001622). The codes used to perform these analyses are available in GitHub: https://github.com/jaqulinwallace/MBL-Morgan-Lab-Analysis.

Statistics

All graphing and statistical analyses were performed using GraphPad Prism 10 (GraphPad Software, La Jolla, CA, USA; RRID:SCR_002798). No outliers were removed from any of the datasets, except for a single CCP/V outlier identified using the ROUT method that was >2.5 SD greater than the mean. Electron microscopy data were generally analysed using a one-way ANOVA, followed by a Tukey's *post hoc* test. Statistical tests of significance are reported for each figure and in the figure legends.

Results

Purification of human multimeric and monomeric α-synuclein from HEK cells

The goal of this study was to determine the specific impacts of multimeric α-synuclein on synaptic vesicle trafficking in comparison to the effects of monomeric α-synuclein, which we previously reported (Banks et al., 2020; Busch et al., 2014; Wallace et al., 2024). We therefore began by expressing and purifying multimeric and monomeric human α-synuclein from HEK 293 cells, given that bacterial cells seem to be unable to facilitate synuclein multimer formation compared to higher eukaryotes (de Boni et al., 2022). Cell lysates obtained after transient expression of α-synuclein were crosslinked *in situ* with

1.43 mM disuccinimidyl glutarate (DSG) and purified using the Strep-tag purification system, followed by size exclusion chromatography (Fig. 1*A*), as described in de Boni et al. (2022). Western blotting showed that HEK-derived α-synuclein multimers ran on a 12% SDS-PAGE gel at around 80 kDa (Fig. 1*B*, left blot). HEK-derived monomeric α-synuclein ran around 14 kDa, similar to *E. coli*-derived monomers, but in a slightly more diffuse pattern, which is probably due to the presence of stochastic covalent attachment of crosslinker (Fig. 1*B*, left blot). Phosphorylation of α-synuclein at serine 129 (pS129) is a post-translational modification that occurs in very low levels in neurons under physiological conditions and builds up in pathological conditions, and this modification modulates α-synuclein functions at synapses (Parra-Rivas et al., 2023; Ramalingam et al., 2023; Wallace et al., 2024). Western blotting using a pS129-specific antibody showed that α-Synuclein purified from HEK cells was not detectably phosphorylated at serine 129 (Fig. 1*B*, right blot). CD spectroscopy revealed that the α-synuclein multimers adopted an alpha-helical structure, as determined by the minima of ellipticity at 208 and 220 nm (Fig. 1*C*). HEK monomers also exhibited a high helical content in solution, unlike *E. coli* derived α-synuclein, which remained unstructured (Fig. 1*C* and *D*) [*E. coli* Monomer: 4.3% (SD 1.2%) helical; HEK Monomer: 43.0% (SD 3.0%) helical; HEK Multimer: 44.0% (SD 2.0%) helical; $n = 3$]. Thus, both HEK-derived monomers and multimers are folded in solution, comparable to the human brain-derived α-synuclein, which we previously reported (Roman-Vendrell et al., 2021).

Acute introduction of multimeric and monomeric α-synuclein impair intracellular vesicle trafficking

To assess how excess multimeric α-synuclein impacts synaptic vesicle trafficking, we utilized as our model the giant RS synapses from the sea lamprey, *Petromyzon marinus* (Fig. 2*A*). Giant RS axons are located within

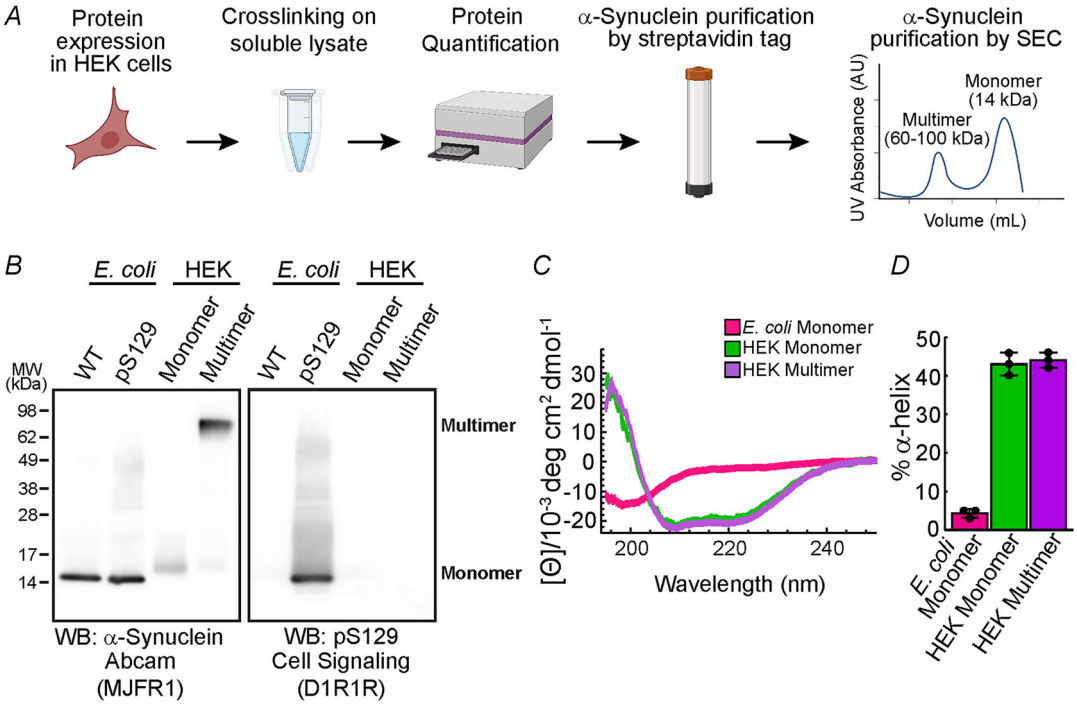

Figure 1. Purification of monomeric and multimeric human α-synuclein from HEK cells
A, streptavidin-tagged α-synuclein was expressed in HEK cells, crosslinked with disuccinimidyl glutarate (DSG) to retain the native structure, and purified on a Strep-trap column. α Synuclein multimers and monomers were separated and purified using size exclusion chromatography (SEC). *B*, left: Western blot showing monomeric α-synuclein (14 kDa) and multimeric α-synuclein (~80 kDa) derived from HEK cells, as well as recombinant wild-type (WT) and phosphoserine 129 (pS129) α-synuclein derived from *E. coli*. α-Synuclein was detected with a rabbit monoclonal anti-α-synuclein antibody (MJFR1, 1:1000). Right: western blot using a pS129-specific α-synuclein antibody (D1R1R, 1:1000) showing that the HEK-derived α-synuclein is not phosphorylated at serine 129. *C* and *D*, circular dichroism spectroscopy revealed that HEK-derived human α-synuclein multimers and monomers both possess an alpha-helical structure in solution, as shown by the minima of ellipticity at 208 and 220 nm. In comparison, recombinant α-synuclein from *E. coli* is largely unfolded in solution. Data shown represent mean with SD from $n = 3$ independent experiments. Diagram in *A* created with BioRender.com.

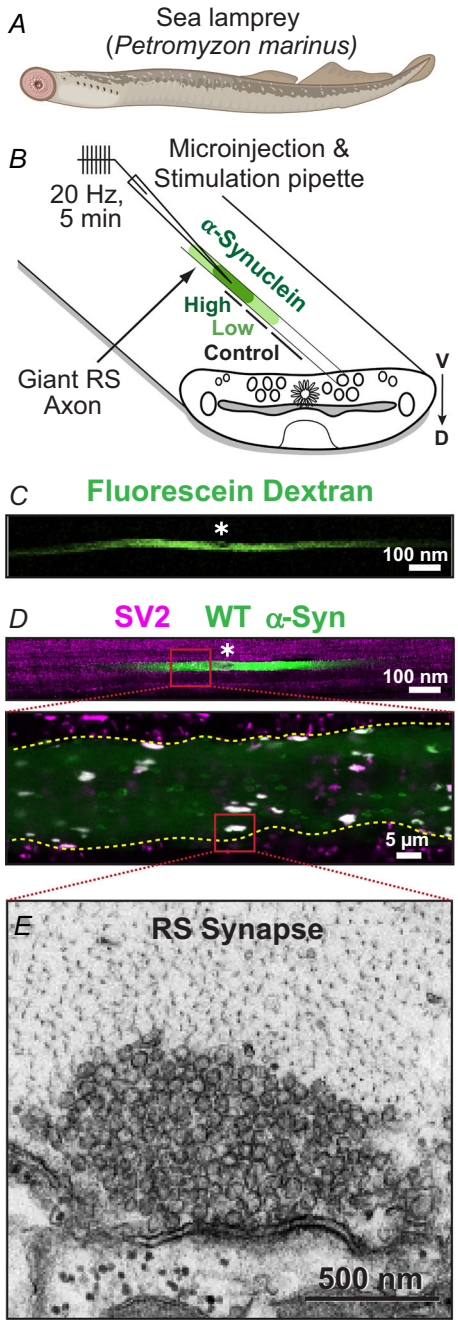

Figure 2. Acute perturbations at lamprey giant reticulospinal (RS) synapses
A, diagram of the sea lamprey (*Petromyzon marinus*), a basal evolved vertebrate. *B*, Lamprey spinal cords were dissected and pinned ventral side up, providing easy access to the giant RS axons for α-synuclein microinjection and action potential stimulation. Diffusion of α-synuclein along the axon generated a concentration gradient, from high concentrations near the injection site to lower concentrations farther away. See Methods and Results sections for more details. V = ventral; D = dorsal. *C*, co-injection of fluorescein dextran (10 kDa) confirmed axonal microinjection. Asterisks in *C* and *D* mark the injection site. *D*, whole mount immunofluorescence against human α-synuclein (green) and synaptic vesicle glycoprotein 2 (SV2; magenta). Colocalization of α-synuclein and SV2 confirmed that the injected α-synuclein (*E. coli*-derived; rPeptide) targeted synapses. Dotted line indicates the borders of a giant RS axon injected with α-synuclein. *E*, Electron micrograph of a lamprey giant RS synapse showing the large vesicle cluster. Figure was partially created with BioRender.com.

the ventromedial tract of the spinal cord. They are exceptionally large (~20–60 µm in diameter), superficial and therefore amenable to acute perturbations of presynaptic processes via axonal microinjection. We previously cloned and sequenced the lamprey synucleins and demonstrated that they are highly conserved with human α-synuclein, expressed endogenously at giant RS synapses and that they phenocopied synaptic effects of human α-synuclein (Busch & Morgan, 2012; Busch et al., 2014; Fouke et al., 2021). For these experiments, the HEK-derived monomeric and multimeric human α-synuclein were separately microinjected into the RS axons, delivering the protein directly to presynapses (Fig. 2*B*–*E*). Co-injection of a fluorescent dye with a comparable molecular weight allowed us to estimate the final α-synuclein concentrations along the injected axon (Fig. 2*B* and *C*). Fluorescein dextran provides useful estimates of reagent diffusion, however, it does not perfectly mirror α-synuclein behaviour, as we have previously shown that *E. coli*-derived α-synuclein preferentially accumulates on presynaptic vesicle clusters (Fig. 2*D*) (Wallace et al., 2024). Starting with multimeric α-synuclein, after injection and diffusion of the protein, we estimate that the final axonal concentration was ~1–2 µM at distances near to the injection site, which we termed the 'high concentration' and ~0.1–0.9 µM at intermediate distances from the injection site, which we termed the 'low concentration'. Synapses located within the injected axon but at a distance beyond the protein diffusion limit served as internal controls. We collected images of synapses from all three regions (Fig. 2*B*), allowing us to determine the dose–response of any effects. Since the normal concentration of α-synuclein at synapses is 3–6 µM (Westphal & Chandra, 2013), the amount of exogenous α-synuclein injected was 0.5- to 2-fold greater than endogenous levels and is commensurate with overexpression levels observed in the brains of PD patients (Miller et al., 2004; Singleton et al., 2003). After α-synuclein injection, the axons were stimulated with action potentials at 20 Hz for 5 min and immediately fixed for electron microscopy. Fixation began at the end of the stimulation period, while continuing to stimulate, and was complete within about 10 s, as determined by cessation of action potentials.

Stimulated control synapses exhibited large synaptic vesicle clusters, shallow plasma membrane evaginations, and a limited number of CCPs and CCVs (Fig. 3*A*). However, after treatment with the low concentration of

multimeric α-synuclein, there was a notable depletion of synaptic vesicles and an increase in the appearance of large vesicular structures, which we call 'cisternae' and are probably a type of endosome (Fig. 3*B*). This phenotype became even more pronounced with higher concentrations of multimeric α-synuclein (Fig. 3*C*). 3D reconstructions generated from five serial micrographs further highlighted the severe loss of synaptic vesicles

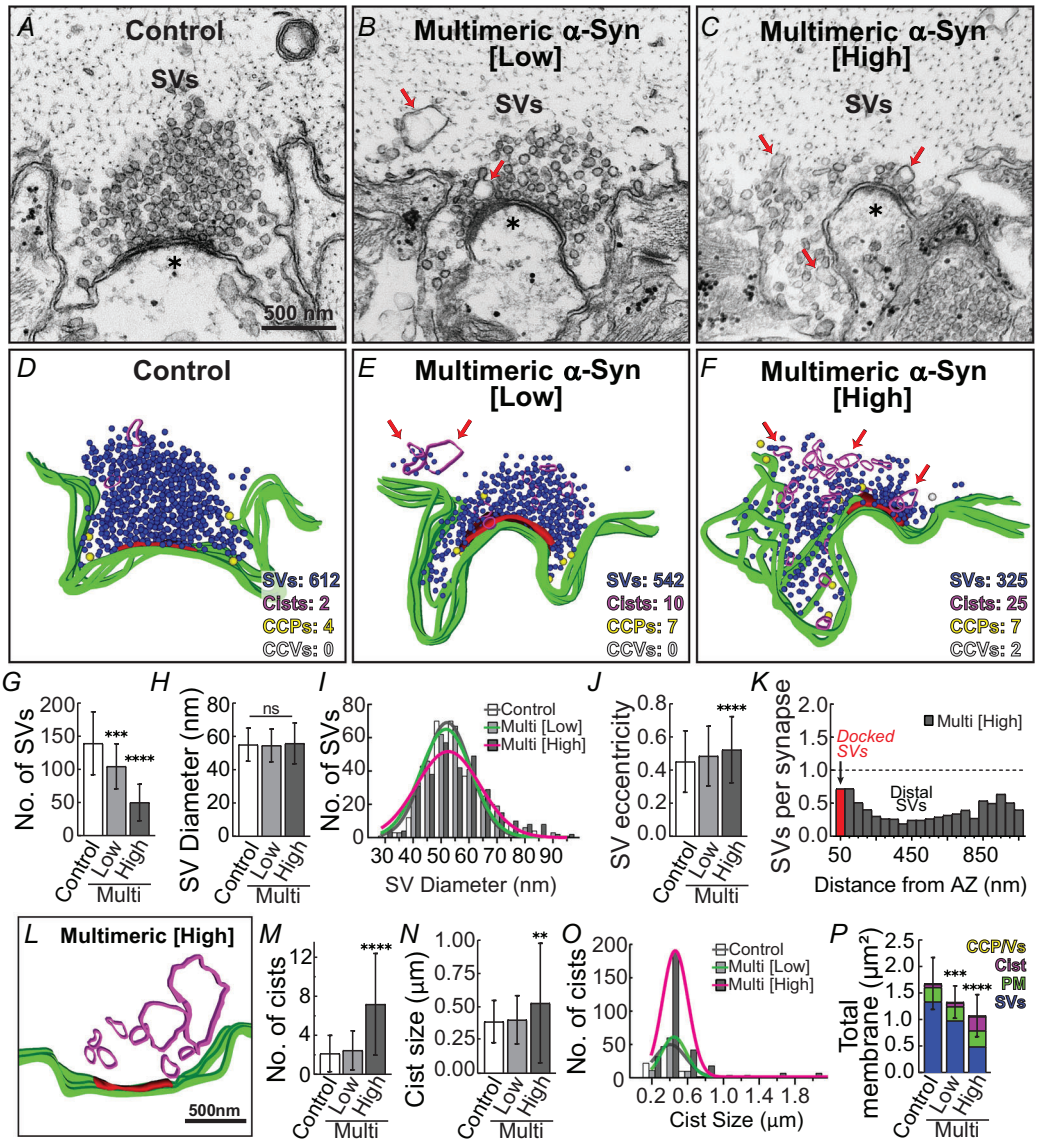

Figure 3. Excess multimeric α-synuclein impairs vesicle trafficking at stimulated lamprey synapses
A–C, electron micrographs showing a progressive, dose-dependent loss of synaptic vesicles (SVs) at stimulated lamprey synapses (20 Hz, 5 min) after introducing multimeric α-synuclein at low (0.1–0.9 μM) or high (1–2 μM) concentrations. Additionally, multimeric α-synuclein increased the number of cisternae, which are presumptive endosomes. Scale bar in *A* applies to *B* and *C*. Asterisks indicate the post-synapse. *D–F*, 3D reconstructions reveal the loss of SVs (blue spheres) and build-up of cisternae (magenta ribbons; see red arrows and L). Green ribbons = plasma membrane (PM); red slab = active zone; yellow and white spheres = clathrin-coated pits and vesicles (CCP*V*s). *G–K*, excess multimeric α-synuclein significantly reduced the number of SVs per synapse. SV depletion occurred throughout the vesicle cluster, including docked and distal vesicle pools. The remaining SVs were of similar size but less circular in shape, as shown by increased eccentricity. AZ = active zone. *L–O*, the loss of SVs was partially compensated for by an increase in the number and size of cisternae. *P*, total membrane analysis revealed a significant loss of synaptic membrane, primarily because of SV depletion. Bars indicate mean with SD from n = 35–39 synapses per condition from N = 3 axons. Asterisks indicate statistical significance compared to control using one-way ANOVA with Tukey's *post hoc* test: $^{**}P = 0.0082$; $^{***}P < 0.001$; $^{****}P < 0.0001$; ns indicates not significant.

and the accumulation of the cisternae caused by excess multimeric α-synuclein (Fig. 3*D*–*F*). We selected images near the center of the synapse, based on active zone morphology, and subsequently performed a quantitative morphometric analysis of all synaptic membranes within a 1 μm radius of the active zone. This analysis revealed that multimeric α-synuclein induced a dose-dependent loss of synaptic vesicles, reaching a 65% decrease in the total synaptic vesicle pool at the high concentration, compared to controls (Fig. 3*G*) [no. of SVs, Control: mean 139 (SD 47) SVs per synapse; $n = 39$ synapses, 3 axons; Multimeric-[Low]: mean 105 (SD 34) SVs per synapse; $n = 35$ synapses; ANOVA $P = 0.0003$; Multimeric-[High]: mean 50 (SD 28) SVs per synapse; $n = 39$ synapses; ANOVA $P < 0.0001$]. The remaining synaptic vesicles had a normal mean diameter and size distribution (Fig. 3*H*, *I*) [SV diameter, Control: mean 55.1 (SD 10) nm; $n = 300$ SVs, 3 axons; Multimeric-[Low]: mean 54.6 (SD 9.9) nm; $n = 300$ SVs, 3 axons; Multimeric-[High]: mean 55.9 (SD 12.3) nm; $n = 300$ SVs, 3 axons; ANOVA $P = 0.6251$]; [Gaussian non-linear fitting, Control: amplitude 69.65, mean 53.19 (SD 8.170); Multimeric-[Low]: amplitude 65.57, mean 52.79 (SD 8.913); Multimeric-[High]: amplitude 52.26, mean 53.45 (SD 11.14)]. At higher concentrations of multimeric α-synuclein, the synaptic vesicles were less circular than in controls, as shown by increased eccentricity (Fig. 3*J*) [SV eccentricity, Control: mean 0.45 (SD 0.19), Multimeric-[Low]: mean 0.49 (SD 0.18), Multimeric-[High]: mean 0.52 (SD 0.20), $n = 300$ SVs, 3 axons per condition, ANOVA $P < 0.0001$]. A vesicle distribution analysis revealed a substantial loss of synaptic vesicles throughout the vesicle cluster, including both docked and distal vesicles (Fig. 3*K*). In parallel, multimeric α-synuclein induced the appearance of large, irregular-shaped cisternae/endosomes, which were not observed at control synapses (Fig. 3*L*). Quantification revealed that multimeric α-synuclein caused a significant increase in the number and size of cisternae/endosomes (Fig. 3*M*–*O*) [no. of Cisternae, Control: mean 2.1 (SD 1.9) cisternae per synapse; $n = 39$ synapses, 3 axons; Multimeric-[Low]: mean 2.5 (SD 2.0) cisternae; $n = 35$ synapses, 3 axons; Multimeric-[High]: mean 7.5 (SD 5.2) cisternae; $n = 39$ synapses, 3 axons; ANOVA $P < 0.0001$] [Cisternae Size, Control: mean 0.39 (SD 0.16) μm; $n = 83$ cisternae, 3 axons; Multimeric-[Low]: mean 0.40 (SD 0.18) μm; $n = 86$ cisternae, 3 axons; Multimeric-[High]: mean 0.53 (SD 0.45) μm; $n = 305$ cisternae, 3 axons; ANOVA $P = 0.0082$]; [Gaussian non-linear fitting, Control: amplitude 48.55, mean 0.3661 (SD 0.1321); Multimeric-[Low]: amplitude 60.01, mean 0.3973 (SD 0.107); Multimeric-[High]: amplitude 189.5, mean 0.4085 (SD 0.1107)]. An analysis of the total membrane area associated with these synaptic membranes combined revealed that the loss of synaptic vesicle membrane was partially compensated for by an increase in the cisternal membrane (Fig. 3*P*). However, there was a significant, 36% loss of total synaptic membrane at high concentrations of multimeric α-synuclein, suggesting that some of the synaptic vesicles probably escaped away from the immediate vicinity of the synapse (Fig. 3*P*) [Total membrane, Control: mean 1.7 (SD 0.5) μm^2; $n = 39$ synapses, 3 axons; Multimeric-[Low]: mean 1.3 (SD 0.3) μm^2; $n = 35$ synapses, 3 axons, ANOVA $P = 0.0010$; Multimeric-[High]: mean 1.1 (SD 0.4) μm^2; $n = 39$ synapses, 3 axons; ANOVA $P < 0.0001$]. Thus, acute introduction of excess multimeric α-synuclein inhibited synaptic vesicle trafficking, leading to a severe loss of vesicles and accumulation of cisternae at the synapse.

For comparison, we also investigated the impacts of acutely introducing HEK-derived monomeric α-synuclein, representing the other α-synuclein species that comprises a minor component in physiological brain-derived α-synuclein (Bartels et al., 2011; Roman-Vendrell et al., 2021). The high concentration of monomeric α-synuclein was estimated at ∼6–12 μM and the low concentration at ∼1–5 μM (see Methods for more details). With respect to the synaptic vesicles and cisternae, excess monomeric α-synuclein caused similar phenotypes to multimeric α-synuclein. There was a gradual, dose-dependent decrease in the number of synaptic vesicles along with a concomitant increase in the number of cisternae (Fig. 4*A*–*F*). At high concentrations, monomeric α-synuclein induced a 56% depletion of synaptic vesicles, compared to controls, including docked and distal SVs (Fig. 4*G*, *K*) [no. of SVs, Control: mean 142 (SD 52) SVs per synapse; Monomeric-[Low]: mean 113 (SD 55) SVs per synapse; Monomeric-[High]: mean 62 (SD 37) SVs per synapse; $n = 26$–32 synapses, 2 axons per condition; ANOVA $P < 0.0001$]. One notable difference was that the remaining synaptic vesicles had slightly larger diameters, resulting in a shift in the peak synaptic vesicle diameter (Fig. 4*H*, *I*) [SV diameter, Control: mean 53.2 (SD 8.4) nm; Monomeric-[Low]: mean 56.7 (SD 8.8) nm, ANOVA $P = 0.0005$; Monomeric-[high]: mean 58.4 (SD 10.4) nm, ANOVA $P < 0.0001$; $n = 200$ SVs, 2 axons per condition]; [Gaussian non-linear fitting, Control: amplitude 64.05, mean 50.98 (SD 5.652); Monomer-[Low]: amplitude 54.71, mean 54.77 (SD 6.925); Monomer-[High]: amplitude 42.85, mean 55.52 (SD 8.887)]. Similar to multimeric α-synuclein, at the higher concentrations of monomeric α-synuclein, the synaptic vesicles were less circular and exhibited increased eccentricity (Fig. 4*J*) [SV eccentricity, Control: mean 0.41 (SD 0.16); Monomeric-[Low]: mean 0.43 (SD 0.18); Monomeric-[High]: mean 0.45 (SD 0.19); $n = 200$ SVs, 2 axons per condition; ANOVA $P = 0.0308$]. Moreover, while monomeric α-synuclein caused an increase in the number of cisternae, there was no significant change in their average size when compared to the controls (Fig. 4*L*–*O*) [no. of Cisternae, Control: mean

1.1 (SD 1.1) cisternae; Monomeric-[Low]: mean 1.5 (SD 1.7) cisternae; Monomeric-[High]: mean 4.6 (SD 3.6) cisternae; n = 26–32 synapses, 2 axons; ANOVA $P < 0.0001$] [Cisternae size, Control: mean 0.39 (SD 0.13) µm; Monomeric-[Low]: mean 0.40 (SD 0.12) µm; Monomeric-[High]: mean 0.47 (SD 0.29) µm; n = 34–147 cisternae, 2 axons per condition; ANOVA $P = 0.2202$]; [Gaussian non-linear fitting, Control: amplitude 21.12, mean 0.3867 (SD 0.4184); Monomeric-[Low]: amplitude 26.02, mean 0.4061 (SD 0.1136); Monomeric-[High]:

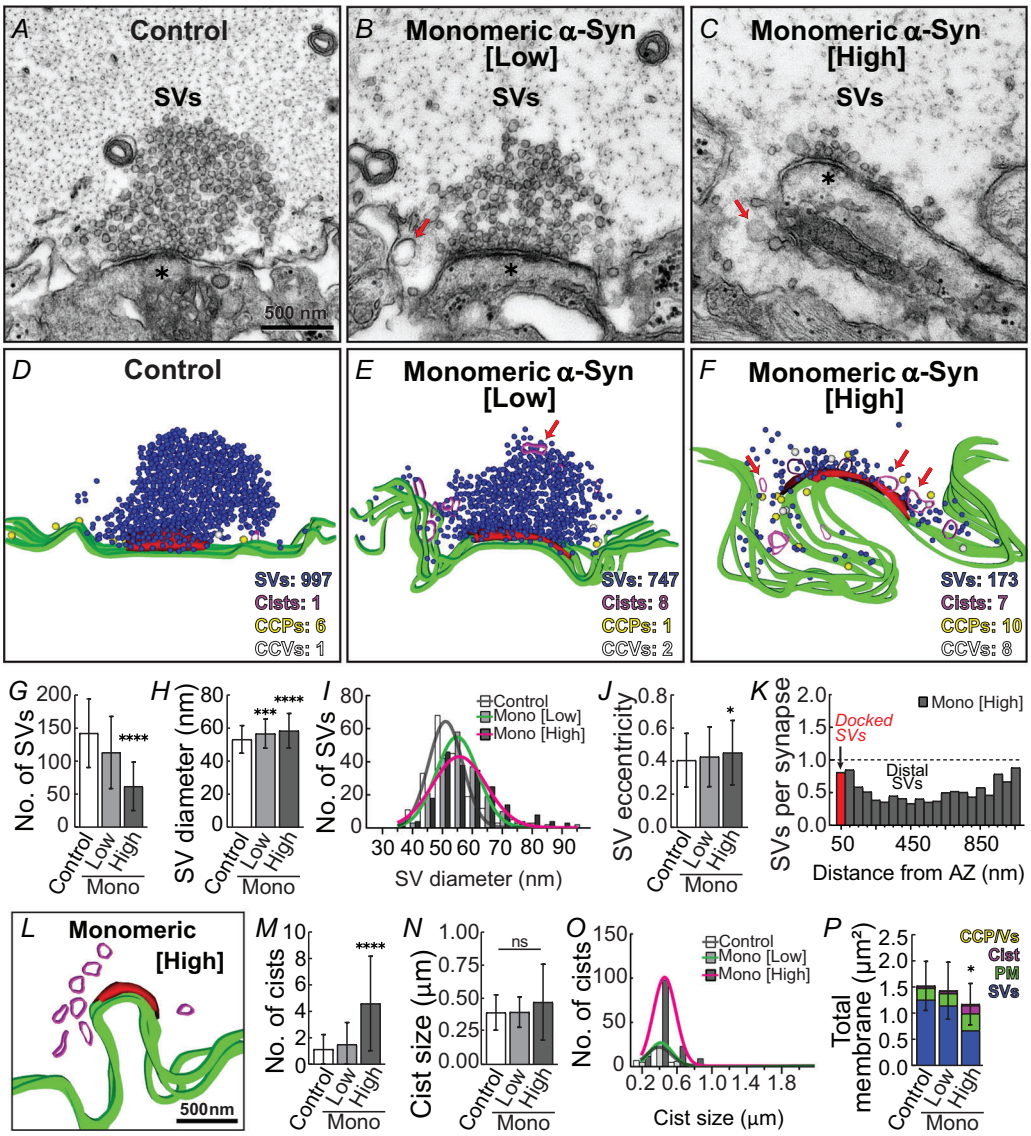

Figure 4. Excess monomeric α-synuclein also impairs vesicle trafficking at stimulated lamprey synapses
A–C, electron micrographs showing a progressive, dose-dependent loss of synaptic vesicles (SVs) at stimulated lamprey RS synapses (20 Hz, 5 min) after introducing monomeric α-synuclein at low (1–5 µM) or high (6–12 µM) concentrations. The cisternae were also more abundant. Scale bar in *A* applies to *B* and *C*. Asterisks indicate the post-synapse. *D–F*, 3D reconstructions revealed the loss of SVs (blue spheres) and accumulation of cisternae (magenta ribbons; see red arrows and L), but also an expansion of the plasma membrane (see also Fig. 5). *G–K*, as with multimeric α-synuclein, excess monomeric α-synuclein significantly reduced the number of SVs throughout the vesicle cluster. However, remaining SVs were significantly larger and less circular in shape. AZ = active zone. *L–O*, the loss of SVs was partially compensated for by an increase in the number of cisternae. Cisternae induced by monomeric α-synuclein were of normal sizes. *P*, total membrane analysis revealed a significant loss of synaptic membrane, primarily due to SV depletion. Bars indicate mean with SD from n = 26–32 synapses per condition from N = 2 axons. Asterisks indicate statistical significance compared to control using one-way ANOVA with Tukey's *post hoc* test: *$P = 0.0308$ in panel *J*; *$P = 0.0121$ in panel *P*; ***$P = 0.0005$; ****$P < 0.0001$; ns indicates not significant.

amplitude 99.43, mean 0.4184 (SD 0.1064)]. Similar to multimeric α-synuclein-treated synapses, at high concentrations of monomeric α-synuclein, there was also a significant, 23% loss of synaptic membrane (Fig. 4*P*) [Total membrane, Control: mean 1.5 (SD 0.5) μm^2; $n = 30$ synapses, 2 axons; Monomeric-[Low]: mean 1.43 (SD 0.5) μm^2; $n = 26$ synapses, 2 axons; Monomeric-[High]: mean 1.2 (SD 0.4) μm^2; $n = 32$ synapses, 2 axons; ANOVA, $P = 0.0121$]. Thus, both multimeric and monomeric α-synuclein had similar impacts on the synaptic vesicle cluster and cisternae with only minor differences in their size distributions, which was expected since these are common features of the synaptic phenotypes that we have observed across multiple α-synuclein species (Banks et al., 2020; Busch et al., 2014; Medeiros et al., 2017; Roman-Vendrell et al., 2021; Wallace et al., 2024).

Excess multimeric and monomeric α-synuclein induce synaptic vesicle declustering

The loss of total synaptic membrane observed with multimeric and monomeric α-synuclein suggested that they induced synaptic vesicle dispersion away from the active zone, as was recently reported for phosphoserine-129 α-synuclein (Wallace et al., 2024). Indeed, synapses treated with high concentrations of either multimeric or monomeric α-synuclein displayed a fragmentation and general dispersion of synaptic vesicles compared to control synapses (Fig. 5*A*–*C*). We performed a nearest-neighbour analysis of synaptic vesicles within 1 μm of the active zone, as previously described (Wallace et al., 2024). After treatment with either multimeric or monomeric α-synuclein, the nearest-neighbour distances between synaptic vesicles increased with distance from the active zone (Fig. 5*D*). This synaptic vesicle declustering was slightly more pronounced for monomeric α-synuclein, as compared to multimeric α-synuclein (Fig. 5*D*) [Control: slope = 0.018 (SD 0.001), $R^2 = 0.02802$, $n = 9503$ SVs [$N = 69$ synapses, 5 axons]; Multimeric-[High]: slope = 0.048 (SD 0.004), $R^2 = 0.05858$, $n = 1924$ SVs [$N = 39$ synapses, 3 axons]; linear regression, ANOVA $P < 0.0001$; and Monomeric-[High]: slope = 0.072 (SD 0.005), $R^2 = 0.1053$, $n = 2002$ SVs [$N = 32$ synapses, 2 axons]; linear regression, one way-ANOVA, $P < 0.0001$]. In addition, the mean distance between synaptic vesicles significantly increased with multimeric and monomeric α-synuclein (Fig. 5*E*) [Distance to

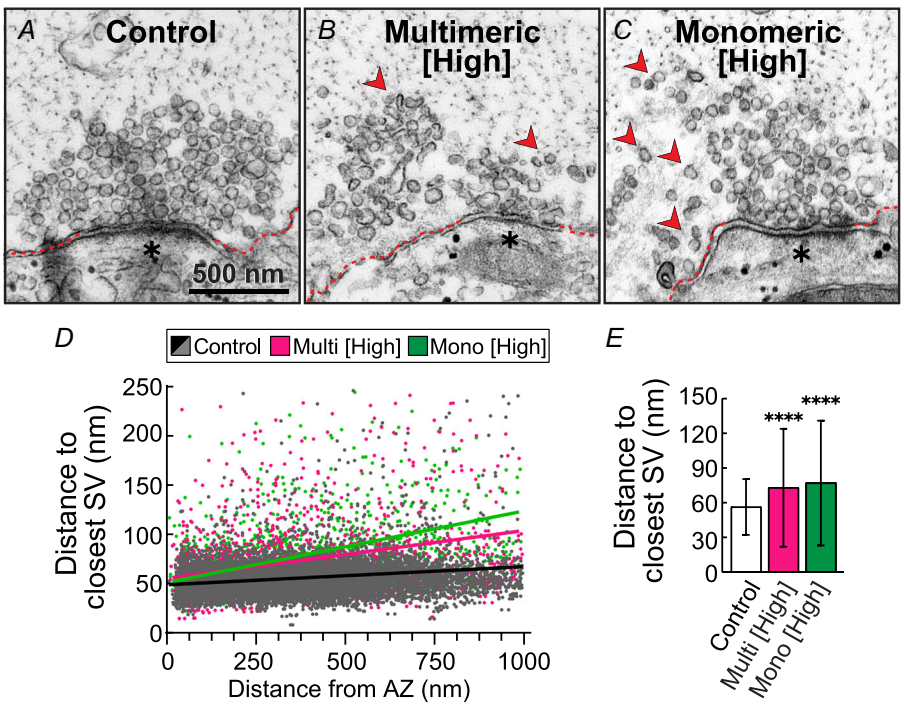

Figure 5. Multimeric and monomeric α-synuclein induced SV declustering at stimulated synapses
A–*C*, compared to control synapses, those treated with high concentrations of multimeric and monomeric α-synuclein exhibited more SV dispersion and declustering away from synapses (arrowheads). Scale bar in *A* applies to *B* and *C*. Asterisks indicate the post-synapse. *D*, a nearest-neighbour analysis revealed that both multimeric and monomeric α-synuclein induced SV declustering, which was progressively worse with increased distance from the active zone (AZ). *E*, monomeric α-synuclein had the greatest effect on SV dispersion. Bars represent mean with SD from n = 1924–9503 SVs from n = 26–69 synapses per condition, N = 2–5 axons. Asterisks indicate statistical significance by one-way ANOVA with Tukey's *post hoc* test: ****$P < 0.0001$.

Closest SV, Control = mean 56.3 (SD 24.2) nm; Multimeric-[High] = mean 72.9 (SD 51.0) nm, ANOVA $P > 0.0001$; Monomeric-[High] = mean 77.0 (SD 54.0) nm, ANOVA $P < 0.0001$]. These findings indicate that multimeric and monomeric α-synuclein additionally induced a declustering of synaptic vesicles during stimulation, causing them to disperse away from the synaptic region, with monomeric α-synuclein having slightly more pronounced effects.

Multimeric and monomeric α-synuclein have distinct effects on synaptic vesicle docking and clathrin-mediated endocytosis at synapses

There were also several clear differences between the synaptic phenotypes induced by excess multimeric and monomeric α-synuclein, specifically regarding the effects on docked vesicles and clathrin-mediated vesicle endocytosis at the plasma membrane. Compared to control synapses, those treated with multimeric α-synuclein exhibited a significant reduction in the number of docked SVs at synapses, which was not the case for monomeric α-synuclein (Fig. 6*A*–*D*) [no. of Docked SVs, Control: mean 4.8 (SD 2.6) docked SVs; $n = 69$ synapses, 5 axons; Multimeric-[High]: mean 3.0 (SD 2.0) docked SVs; $n = 39$ synapses, 3 axons, ANOVA $P = 0.0010$; Monomeric-[High]: mean 4.0 (SD 2.6); $n = 32$ synapses, 2 axons]. To further assess this, we measured the density of docked vesicles, that is the number of docked SVs per micrometre length of active zone. Across experimental conditions, the active zone lengths were not significantly different (Fig. 6*E*) [Active Zone Length, Control: mean 0.6 (SD 0.2) µm; Multimeric-[High]: mean 0.7 (SD 0.2) µm; Monomeric-[High]: mean 0.7 (SD 0.3) µm; $n = 32$–69 synapses, 2–5 axons per condition; ANOVA $P = 0.7188$]. These analyses confirmed that only multimeric α-synuclein caused a significant reduction in the density of docked SVs at the active zones compared to controls (Fig. 6*F*) [Density of Docked SVs, Control: mean 7.4 (SD 4.0) SVs/µm; Multimeric-[High]: mean 4.6 (SD 3.1) SVs/µm; Monomeric-[High]: mean 6.2 (SD 4.2) SVs/µm; $n = 32$–69 synapses, 2–5 axons per condition; ANOVA $P = 0.0012$].

While multimeric α-synuclein reduced SV docking, conversely, only monomeric α-synuclein had substantial impacts on synaptic vesicle endocytosis events at the plasma membrane. Compared to control synapses, multimeric α-synuclein caused only modest changes to the plasma membrane evaginations and clathrin-coated pits and vesicles (CCP/Vs) (Fig. 7*A*–*B*, *D*–*E*). In contrast, monomeric α-synuclein induced deep plasma membrane

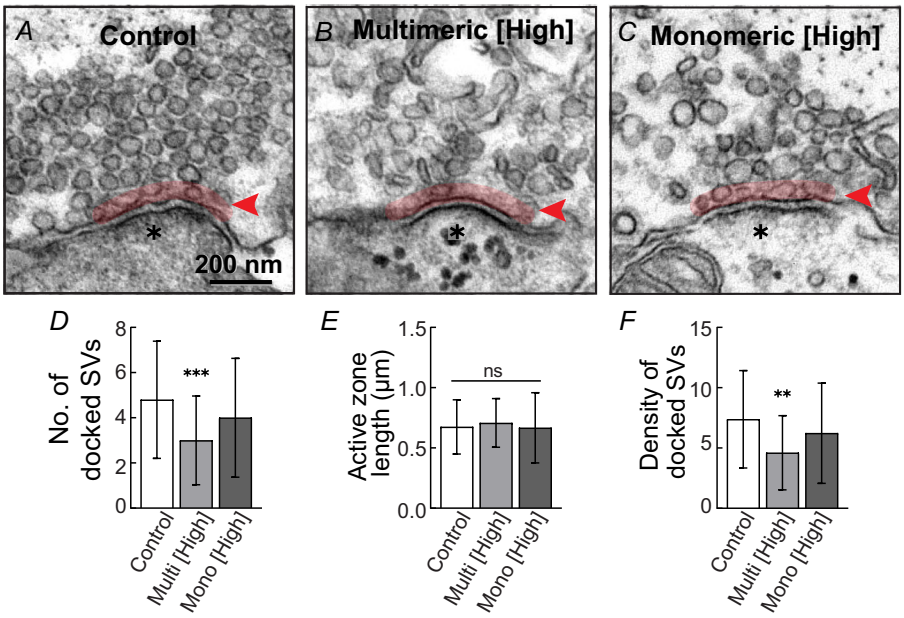

Figure 6. Multimeric α-synuclein reduces the density of docked vesicles
A–*C*, micrographs showing a reduction in the number of docked vesicles (red highlight) in the presence of multimeric α-synuclein. Docked vesicles are defined as being within 50 nm of the active zone, measured from the centre of the synaptic vesicle (SV) to the midpoint of the active zone. *D*, only multimeric α-synuclein significantly decreased the number of docked vesicles. *E*, the lengths of the active zones were not significantly different between experimental conditions. *F*, the density of docked vesicles, calculated as the number of docked SVs per micrometre of active zone length, was reduced in the presence of multimeric α-synuclein. Bars represent mean with SD from n = 26–69 synapses per condition, N = 2–5 axons. Asterisks indicate statistical significance by one-way ANOVA with Tukey's *post hoc* test: $^{**}P = 0.0012$; $^{***}P = 0.0010$; ns indicates not significant.

evaginations and a greater number of CCP/Vs (Fig. 7*C*, *F*). Plasma membrane evaginations were significantly larger with monomeric α-synuclein, compared to multimeric α-synuclein and controls (Fig. 7*G*) [Plasma membrane, Control: mean 1.82 (SD 0.46) µm; Multimeric-[High]: mean 2.15 (SD 0.99) µm; Monomeric-[High]: mean 2.32 (SD 0.97) µm; n = 32–69 synapses, 2–5 axons (2–5 animals); ANOVA P = 0.0074]. Similarly, only monomeric α-synuclein led to a significant increase in the total number of CCP/Vs per synapse, whereas multimeric α-synuclein did not (Fig. 7*H*) [Total no. of Clathrin Coats, Control: mean 1.5 (SD 1.1) coats; Multimeric-[High]: mean 1.8 (SD 2.1) coats; Monomeric-[High]; mean 2.4 (SD 1.7) coats; n = 32–69 synapses, 2–5 axons/animals; ANOVA P = 0.0159]. Specifically, there was a significant increase in the clathrin-coated pits with constricted necks (Stage 3), suggesting an impairment of vesicle fission (Fig. 7*I–J*) [no. of Clathrin Coats, Stage 1-Control: mean 0.22 (SD 0.45) CCPs; Multimeric-[High]: mean 0.08 (SD 0.27) CCPs; Monomeric-[High]: mean 0.19 (SD 0.40) CCPs; ANOVA P = 0.9334; Stage 2-Control: mean 0.35 (SD 0.48) CCPs; Multimeric-[High]: mean 0.39 (SD 0.68) CCPs; Monomeric-[High]: mean 0.22 (SD 0.42) CCPs; ANOVA P = 0.4920; Stage 3-Control: mean 0.54 (SD 0.63) CCPs; Multimeric-High: mean 0.61 (SD 0.89) CCPs; Monomeric-[High]: mean 1.25 (SD 1.11) CCPs; ANOVA: P = 0.0003; Stage 4-Control: mean 0.36 (SD 0.59) CCVs; Multimeric-[High]: mean 0.76 (SD 1.20) CCVs; Monomeric-[High]: mean 0.75 (SD 0.8) CCVs; ANOVA P = 0.0542]. Thus, while HEK-derived

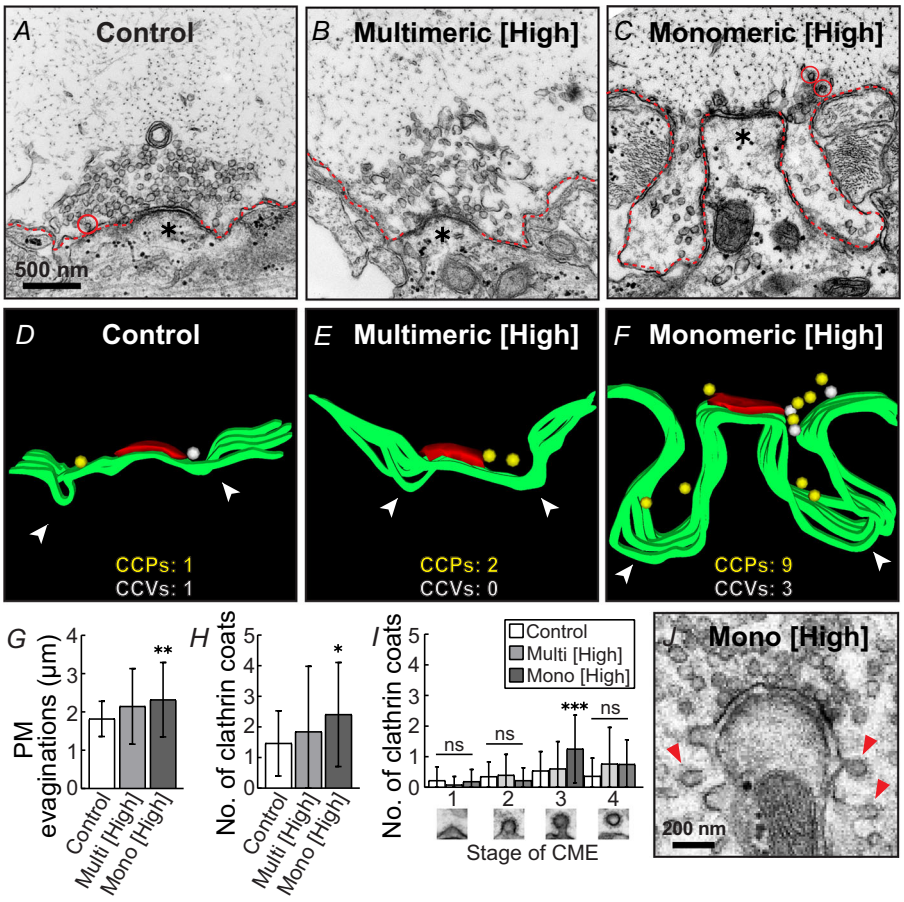

Figure 7. Monomeric α-synuclein distinctly impaired clathrin-mediated SV endocytosis from the plasma membrane
A–C, synapses treated with monomeric α-synuclein had larger plasma membrane evaginations (dotted lines) and more clathrin-coated pits and vesicles (CCP/Vs; circles) than control or multimer-treated synapses. *D–F*, 3D reconstructions with the vesicular structures removed clearly show the extended PM evaginations (green ribbons; arrowheads) and abundant CCP/Vs (yellow and white spheres) induced after treatment with monomeric α-synuclein. *G* and *H*, PM evaginations and total number of clathrin coats were significantly increased only with excess monomeric α-synuclein. *I* and *J*, monomeric α-synuclein selectively increased CCPs with constricted necks (stage 3), indicating an inhibition of vesicle fission (see arrows in *J*). Bars represent mean with SD from n = 26–69 synapses per condition, N = 2–5 axons. Asterisks indicate statistical significance by one-way ANOVA with Tukey's *post hoc* test: *P = 0.0159; **P = 0.0074; ***P = 0.0003; ns indicates not significant.

monomeric α-synuclein impaired clathrin-mediated endocytosis at the plasma membrane, as previously reported for *E. coli*-derived α-synuclein (Banks et al., 2020; Busch et al., 2014; Medeiros et al., 2017), in contrast, multimeric α-synuclein had minimal impacts on plasma membrane events.

HEK-derived monomeric α-synuclein induces atypical fusion/fission events at the active zone

In line with the observation that excess monomeric α-synuclein impacted vesicle trafficking events at the plasma membrane, monomeric α-synuclein also induced large, atypical structures at the active zone, which were fused and therefore contiguous with the plasma membrane (Fig. 8). We termed these structures 'fusosomes' (Roman-Vendrell et al., 2021). Many fusosomes appeared as large cisternae attached to the plasma membrane, some of which had CCPs emanating from them, while others looked more like tubules comprising multiple fused vesicles (Fig. 8*A*). These structures were completely absent from stimulated, control synapses, and were more prevalent with monomeric α-synuclein than multimeric α-synuclein (Fig. 8*B*) [no. of Fusosomes, Control: mean 0 (SD 0) fusosomes per synapse, $n = 69$ synapses; Multimeric-[High] = mean 0.03 (SD 0.16) fusosomes per synapse, $n = 39$ synapses; Monomeric-[High] = mean 0.28 (SD 0.52) fusosomes per synapse, $n = 32$ synapses; one-way ANOVA, $P < 0.0001$]. The fusosomes were observed both near the centre and at the periphery of the active zone (Fig. 8*C*). While the precise nature of the fusosomes remains unclear, their presence further underscores the impacts of monomeric α-synuclein on the plasma membrane.

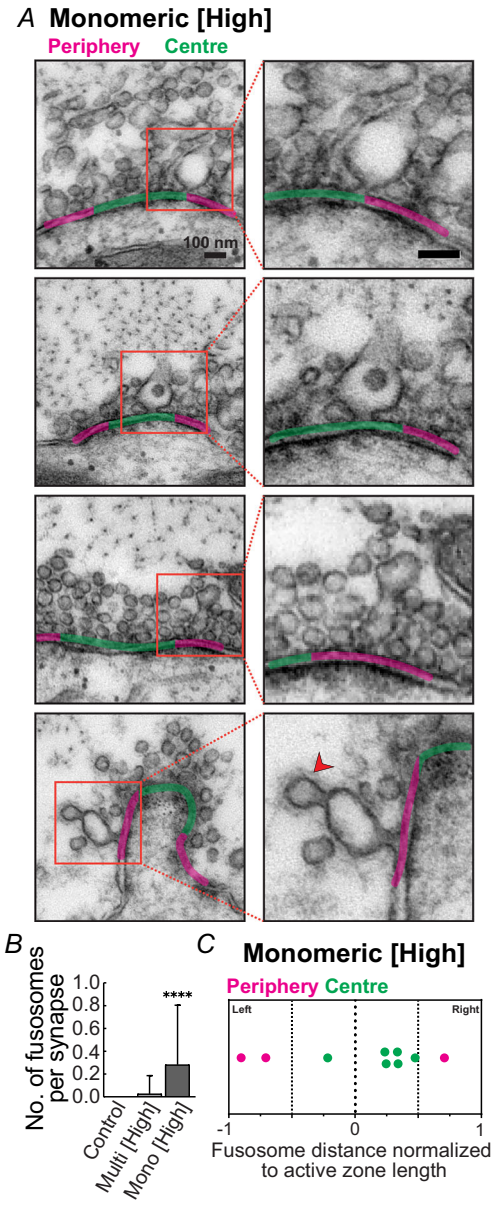

Figure 8. Monomeric α-synuclein produced abnormal fusion/fission events
A, electron micrographs showing the localization and different morphologies of 'fusosomes' induced by excess monomeric α-synuclein, all of which are contiguous with the active zone membrane. Arrowhead indicates CCPs emanating from some fusosomes. Scale bar = 100 nm. *B*, quantification of fusosomes revealed a significant increase in these structures only at synapses treated with monomeric α-synuclein. *C*, Fusosomes were observed both near the centre and at the periphery of active zones. Data represent mean with SD from $n = 32$–69 synapses per condition from $N = 2$–5 axons. Asterisks indicate statistical significance by one-way ANOVA with Tukey's *post hoc* test: ****$P < 0.0001$.

Discussion

Taken together, the data presented here provide additional evidence that different molecular species of α-synuclein produce overlapping but also distinct impacts on synaptic vesicle trafficking (Fig. 9). For both multimeric and monomeric α-synuclein, the inhibition of local synaptic vesicle trafficking was evidenced by a loss of synaptic vesicles, which was partially compensated for by an increase in endocytic intermediates. In addition, the loss of total synaptic membrane may be explained by the synaptic vesicle declustering/reclustering defects we observed for both α-synuclein species (Fig. 9*B*–*C*). Multimeric and monomeric α-synuclein also induced a significant increase in the number of 'cisternae' at synapses, suggesting that α-synuclein impairs synaptic vesicle re-formation from vesicular endosomes.

Despite these similarities, distinct phenotypes emerged between the two forms of α-synuclein. Multimeric

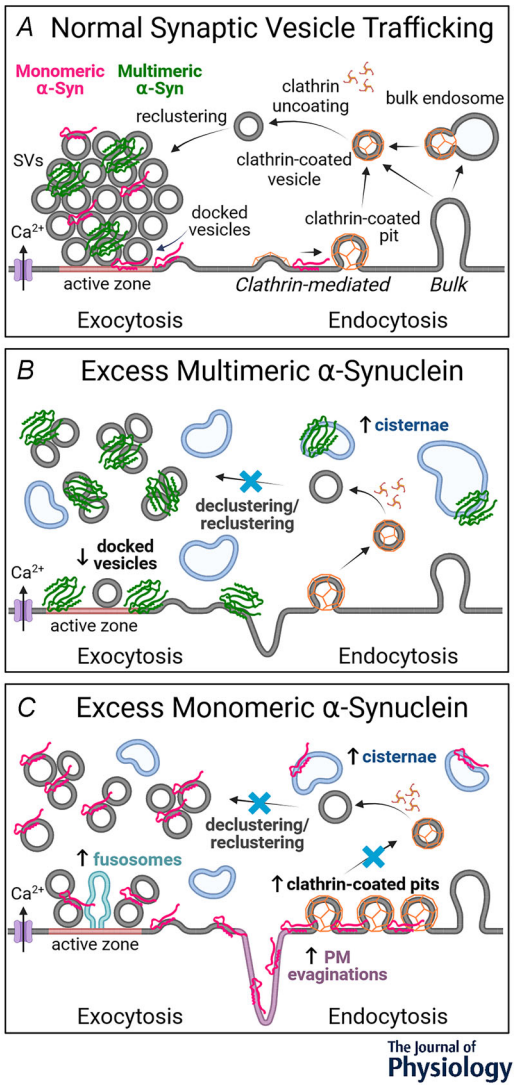

Figure 9. Working model illustrating how multimeric and monomeric α-synuclein impact synapses
A, under physiological conditions, α-synuclein regulates synaptic vesicle (SV) exocytosis, endocytosis and SV clustering at presynaptic terminals. Physiological α-synuclein comprises multimeric and monomeric α-synuclein. Lamprey synapses utilize both clathrin-mediated and bulk endocytosis for SV recycling, though non-clathrin mechanisms may also be involved. *B*, when introduced acutely to synapses, excess multimeric α-synuclein disrupts normal SV trafficking, resulting in a loss of SVs. It impairs SV declustering/reclustering, and reduces vesicle docking at the active zone. Additionally, multimeric α-synuclein promotes the formation of cisternae, indicating a disruption in endosomal vesicle trafficking. These perturbations likely impair synaptic transmission. *C*, similarly, excess monomeric α-synuclein also induces SV declustering/reclustering defects and induces the formation of atypical cisternae. while also uniquely inhibiting clathrin-mediated endocytosis, leading to an accumulation of clathrin-coated pits, plasma membrane evaginations and consequently fewer recycled synaptic vesicles. Monomeric α-synuclein also promotes the formation of aberrant 'fusosomes' at the active zone. Created with BioRender.com.

α-synuclein appears to uniquely impair synaptic vesicle docking, which may explain the modest impact on the plasma membrane. This suggests that synaptic vesicles fail to dock or fuse properly in the presence of multimeric α-synuclein, preventing their buildup at the membrane. In contrast, only monomeric α-synuclein inhibited clathrin-mediated synaptic vesicle endocytosis and consequently induced a greater expansion of the plasma membrane (Fig. 9*C*). Monomeric α-synuclein also induced fusosomes at the active zone (Fig. 9*C*). While the identity of these structures remains to be determined, they could be recycling or bulk endosomes that are aberrantly fusing with or budding from the active zone, or alternatively a consequence of multivesicular fusion events.

The synaptic phenotypes we report here are specific for α-synuclein since injection of other similar-sized inert proteins (e.g. GST) or synaptic chaperones (e.g. Hsc70) had little to no impact on synaptic morphology under the same conditions (Banks et al., 2020; Busch et al., 2014). Moreover, with low-frequency stimulation (5 Hz), or in the absence of stimulation, excess human α-synuclein has little to no effect on synaptic morphology, indicating an activity-dependent effect while also ruling out artifacts due to microinjection damage (Busch et al., 2014; Wallace et al., 2024). Finally, we have previously shown that injection of size exclusion chromatography samples immunodepleted of α-synuclein had no effect on synapses, ruling out any effects of the eluate constituents (Roman-Vendrell et al., 2021). Thus, the synaptic phenotypes reported here are highly specific for excess α-synuclein at stimulated synapses and are in line with results from our prior studies, as will be discussed in more detail below.

Using the lamprey synapse model, we had previously reported that recombinant *E. coli*-derived monomeric and dimeric α-synuclein impaired slightly different stages of clathrin-mediated endocytosis with monomeric α-synuclein impairing the uncoating of CCVs and dimeric α-synuclein impairing an earlier stage of vesicle fission from the plasma membrane (Banks et al., 2020; Medeiros et al., 2017, 2018). In contrast, human brain-derived α-synuclein, which was obtained from a neuropathologically normal patient, predominantly affected intracellular vesicle trafficking with minimal impacts on the plasma membrane (Roman-Vendrell et al., 2021). The human brain-derived α-synuclein used in our prior study comprised a mixture of predominantly multimeric α-synuclein with a minor component of monomeric α-synuclein. Given that the purified HEK-derived multimeric α-synuclein used in this study produced very similar effects on synaptic vesicle trafficking, we can now conclude that the synaptic phenotype caused by acute introduction of excess human brain-derived α-synuclein largely arose

from the multimeric α-synuclein, specifically α-synuclein tetramers and other related oligomers with molecular weights ranging from 60 to 100 kDa (Roman-Vendrell et al., 2021). However, the appearance of 'fusosomes' observed with brain-derived α-synuclein was probably due to the minor component of monomeric α-synuclein present in those samples (Roman-Vendrell et al., 2021). Taken together, these findings underscore the complexity of phenotypes induced by accumulation of α-synuclein in neurons and the need to determine the selective impacts of different molecular species and conformations on the physiology and cell biology of synapses. In the future, it will be important to determine how higher molecular weight α-synuclein oligomers impact synapses, including α-synuclein strains and conformations derived from patients with PD and DLB (de Boni et al., 2022; Sanderson et al., 2020).

Another observation resulting from this study is that the source of α-synuclein may also be a factor that influences its bioactivity and therefore the cellular phenotypes observed. We previously reported that *E. coli*-derived recombinant monomeric α-synuclein impaired clathrin-mediated synaptic vesicle endocytosis by inhibiting clathrin uncoating, leading to an abundance of free CCVs within the synaptic vicinity (Banks et al., 2020; Medeiros et al., 2017). In comparison, HEK-derived monomeric α-synuclein also inhibited clathrin-mediated synaptic vesicle recycling from the plasma membrane (Fig. 7). However, HEK-derived monomeric α-synuclein seemed to preferentially impair CCP fission from the plasma membrane (Fig. 7*I*), similar to the effects of *E. coli*-derived α-synuclein dimers (Banks et al., 2020; Medeiros et al., 2017). Additionally, α-synuclein-112, a splice variant with enhanced dimerization on synaptic membranes, also impaired CCP fission (Soll et al., 2020). Thus, the CCP fission defect leads us to speculate that the HEK-derived monomers may be dimerizing on membranes upon entering the synaptic environment. Other possibilities underlying these phenotypic differences may include their distinct structures (Fig. 1) or the N-acetylation that occurs on all mammalian proteins (Bartels et al., 2011; Burre et al., 2013; Fauvet, Mbefo et al., 2012; Theillet et al., 2016). N-acetylation can increase the helical propensity of α-synuclein (Bartels et al., 2014; Fauvet, Fares et al., 2012; Kang et al., 2012; Maltsev et al., 2012) and impact its lipid-binding properties either directly or indirectly by interacting with different synaptic partners (Iyer et al., 2016; Runfola et al., 2020). Notably, a recent study has shown that this post-translational modification enhances α-synuclein's role in mediating synaptic vesicle clustering *in vitro* (Wang et al., 2024). Overall, despite the differences in structures with *E. coli* being unfolded and mammalian cell-derived monomeric α-synuclein being folded in solution (Fig. 1), the synaptic phenotypes were remarkably similar. This further implies that *in vivo* membrane binding of *E. coli* and HEK-derived monomeric α-synuclein was very similar, since many studies have now shown that synaptic localization, synaptic phenotypes and neuronal toxicity are all highly correlated with the membrane binding properties of α-, β- and γ-synucleins, and numerous α-synuclein variants (Burre et al., 2012; Busch et al., 2014; Carnazza et al., 2022; Nemani et al., 2010; Soll et al., 2020).

Going forward, it will be important to determine any differences in the biochemical or biological activities commensurate with the structural properties of α-synuclein, whether it is monomeric or multimeric, helical or unfolded (Burre et al., 2014; Selkoe et al., 2014; Wang et al., 2014). However, this could be quite challenging, given that the types of biochemical analyses needed to assess these distinctions require large amounts of protein that are easily purified from bacteria, but not from HEK cells or limited human brain samples. Moreover, our attempts to accurately quantify the *in situ* concentration of the microinjected HEK-derived monomeric and multimeric α-synuclein via immunofluorescence have been more challenging compared to *E. coli*-derived material, possibly due to a difference in epitope exposure between the folded and unfolded species. We are thereby limited in a detailed examination of their levels within axons and/or synapses that could provide additional insights into their biological activities. However, we know that recombinant wild-type α-synuclein and phosphoserine 129 α-synuclein preferentially accumulate on presynaptic vesicle clusters (Fig. 2*C*) (Wallace et al., 2024). Furthermore, the electron microscopy phenotypes reported here for both multimeric and monomeric α-synuclein indicate strong impacts on the synaptic vesicle clusters and synaptic vesicle morphologies themselves, indicating that the synaptic vesicles are a primary target of the injected α-synuclein (Figs 3–6). Nonetheless, understanding any differences in the behaviour of monomeric versus multimeric human α-synuclein should remain a goal for future experiments, as this could reveal important and novel biological activities of α-synuclein, depending on the cellular context from which it was derived.

Finally, our data further support the model that accumulation of monomeric α-synuclein in neurons leads to the greatest cellular toxicity. Point mutations in α-synuclein that destabilize physiological α-synuclein tetramers and increase monomeric content induce aggregation and cause greater toxicity in mammalian cell lines and α-synuclein rodent models (Dettmer, Newman, Soldner et al., 2015, Dettmer, Newman, von Saucken et al., 2015, 2017). Moreover, in the brains of sporadic PD and DLB patients, the equilibrium of α-synuclein conformations is shifted from physiological α-synuclein multimers in favour of monomers, suggesting this as

a mechanism underlying the disease pathology (de Boni et al., 2022). Here, we also showed that monomeric α-synuclein caused more dramatic impacts on synaptic vesicle trafficking than equimolar amounts of multimeric α-synuclein. Specifically, in addition to the buildup of 'cisternae' (endosomes) that also occurred at multimer-treated synapses, monomeric α-synuclein caused greater synaptic vesicle declustering (Fig. 5), impaired clathrin-mediated endocytosis from the plasma membrane (Fig. 7) and induced atypical fusion/fission events at the active zone (Fig. 8) (Banks et al., 2020; Medeiros et al., 2017; Roman-Vendrell et al., 2021). We recently reported that excess monomeric α-synuclein also greatly reduced FM1-43 destaining kinetics at lamprey synapses relative to controls, indicating that these morphological effects are ultimately linked to a severe impairment of functional synaptic vesicle exo/endocytosis (Wallace et al., 2024). Although acutely increasing the levels of multimeric α-synuclein – or any α-synuclein species – disrupts synapses, our current results collectively suggest that synapses are most negatively affected by high levels of monomeric α-synuclein. In summary, these findings emphasize the importance of understanding how distinct α-synuclein species, including their post-translational modifications (Anderson et al., 2006; Bell et al., 2023), differentially affect synaptic organelles, as the affected organelles and their molecular interactors represent cellular targets for therapeutic interventions in PD, DLB and other synucleinopathies.

References

Ajmani, N., Yasmin, T., Docker, M. F., & Good, S. V. (2021). Transcriptomic analysis of gonadal development in parasitic and non-parasitic lampreys (*Ichthyomyzon* spp.), with a comparison of genomic resources in these non-model species. *G3 Genes|Genomes|Genetics*, **11**(2), jkab030.

Anderson, J. P., Walker, D. E., Goldstein, J. M., de Laat, R., Banducci, K., Caccavello, R. J., Barbour, R., Huang, J., Kling, K., Lee, M., Diep, L., Keim, P. S., Shen, X., Chataway, T., Schlossmacher, M. G., Seubert, P., Schenk, D., Sinha, S., Gai, W. P., & Chilcote, T. J. (2006). Phosphorylation of Ser-129 is the dominant pathological modification of alpha-synuclein in familial and sporadic Lewy body disease. *Journal of Biological Chemistry*, **281**(40), 29739–29752.

Banks, S. M. L., Medeiros, A. T., McQuillan, M., Busch, D. J., Ibarraran-Viniegra, A. S., Sousa, R., Lafer, E. M., & Morgan, J. R. (2020). Hsc70 ameliorates the vesicle recycling defects caused by excess alpha-synuclein at synapses. *eNeuro*, **7**(1), https://doi.org/10.1523/ENEURO.0448-19.2020

Bartels, T., Choi, J. G., & Selkoe, D. J. (2011). alpha-Synuclein occurs physiologically as a helically folded tetramer that resists aggregation. *Nature*, **477**(7362), 107–110.

Bartels, T., Kim, N. C., Luth, E. S., & Selkoe, D. J. (2014). N-alpha-acetylation of alpha-synuclein increases its helical folding propensity, GM1 binding specificity and resistance to aggregation. *PLoS ONE*, **9**(7), e103727.

Bell, R., Castellana-Cruz, M., Nene, A., Thrush, R. J., Xu, C. K., Kumita, J. R., & Vendruscolo, M. (2023). Effects of N-terminal acetylation on the aggregation of disease-related alpha-synuclein variants. *Journal of Molecular Biology*, **435**(1), 167825.

Bendor, J. T., Logan, T. P., & Edwards, R. H. (2013). The function of alpha-synuclein. *Neuron*, **79**(6), 1044–1066.

Bridi, J. C., & Hirth, F. (2018). Mechanisms of alpha-synuclein induced synaptopathy in Parkinson's disease. *Frontiers in Neuroscience*, **12**, 80.

Burre, J., Sharma, M., & Sudhof, T. C. (2012). Systematic mutagenesis of alpha-synuclein reveals distinct sequence requirements for physiological and pathological activities. *Journal of Neuroscience*, **32**(43), 15227–15242.

Burre, J., Sharma, M., & Sudhof, T. C. (2014). alpha-Synuclein assembles into higher-order multimers upon membrane binding to promote SNARE complex formation. *Proceedings of the National Academy of Sciences of the United States of America*, **111**, E4274–4283.

Burre, J., Vivona, S., Diao, J., Sharma, M., Brunger, A. T., & Sudhof, T. C. (2013). Properties of native brain alpha-synuclein. *Nature*, **498**(7453), E4–E6. discussion E6-7.

Busch, D. J., & Morgan, J. R. (2012). Synuclein accumulation is associated with cell-specific neuronal death after spinal cord injury. *Journal of Comparative Neurology*, **520**(8), 1751–1771.

Busch, D. J., Oliphint, P. A., Walsh, R. B., Banks, S. M., Woods, W. S., George, J. M., & Morgan, J. R. (2014). Acute increase of alpha-synuclein inhibits synaptic vesicle recycling evoked during intense stimulation. *Molecular Biology of the Cell*, **25**(24), 3926–3941.

Carnazza, K. E., Komer, L. E., Xie, Y. X., Pineda, A., Briano, J. A., Gao, V., Na, Y., Ramlall, T., Buchman, V. L., Eliezer, D., Sharma, M., & Burre, J. (2022). Synaptic vesicle binding of alpha-synuclein is modulated by beta- and gamma-synucleins. *Cell Reports*, **39**(2), 110675.

Chandra, S., Chen, X., Rizo, J., Jahn, R., & Sudhof, T. C. (2003). A broken alpha -helix in folded alpha -Synuclein. *Journal of Biological Chemistry*, **278**(17), 15313–15318.

de Boni, L., Watson, A. H., Zaccagnini, L., Wallis, A., Zhelcheska, K., Kim, N., Sanderson, J., Jiang, H., Martin, E., Cantlon, A., Rovere, M., Liu, L., Sylvester, M., Lashley, T., Dettmer, U., Jaunmuktane, Z., & Bartels, T. (2022). Brain region-specific susceptibility of Lewy body pathology in synucleinopathies is governed by alpha-synuclein conformations. *Acta Neuropathologica*, **143**(4), 453–469.

Dettmer, U., Newman, A. J., Soldner, F., Luth, E. S., Kim, N. C., von Saucken, V. E., Sanderson, J. B., Jaenisch, R., Bartels, T., & Selkoe, D. (2015). Parkinson-causing alpha-synuclein missense mutations shift native tetramers to monomers as a mechanism for disease initiation. *Nature Communications*, **6**(1), 7314.

Dettmer, U., Newman, A. J., von Saucken, V. E., Bartels, T., & Selkoe, D. (2015). KTKEGV repeat motifs are key mediators of normal alpha-synuclein tetramerization: Their mutation causes excess monomers and neurotoxicity. *Proceedings of the National Academy of Sciences of the United States of America*, **112**(31), 9596–9601.

Dettmer, U., Ramalingam, N., von Saucken, V. E., Kim, T. E., Newman, A. J., Terry-Kantor, E., Nuber, S., Ericsson, M., Fanning, S., Bartels, T., Lindquist, S., Levy, O. A., & Selkoe, D. (2017). Loss of native alpha-synuclein multimerization by strategically mutating its amphipathic helix causes abnormal vesicle interactions in neuronal cells. *Human Molecular Genetics*, **26**(18), 3466–3481.

Eguchi, K., Taoufiq, Z., Thorn-Seshold, O., Trauner, D., Hasegawa, M., & Takahashi, T. (2017). Wild-type monomeric alpha-synuclein can impair vesicle endocytosis and synaptic fidelity via tubulin polymerization at the calyx of held. *Journal of Neuroscience*, **37**(25), 6043–6052.

Fauvet, B., Fares, M. B., Samuel, F., Dikiy, I., Tandon, A., Eliezer, D., & Lashuel, H. A. (2012). Characterization of semisynthetic and naturally Nalpha-acetylated alpha-synuclein in vitro and in intact cells: Implications for aggregation and cellular properties of alpha-synuclein. *Journal of Biological Chemistry*, **287**(34), 28243–28262.

Fauvet, B., Mbefo, M. K., Fares, M. B., Desobry, C., Michael, S., Ardah, M. T., Tsika, E., Coune, P., Prudent, M., Lion, N., Eliezer, D., Moore, D. J., Schneider, B., Aebischer, P., El-Agnaf, O. M., Masliah, E., & Lashuel, H. A. (2012). alpha-Synuclein in central nervous system and from erythrocytes, mammalian cells, and Escherichia coli exists predominantly as disordered monomer. *Journal of Biological Chemistry*, **287**(19), 15345–15364.

Fiala, J. C. (2005). Reconstruct: A free editor for serial section microscopy. *Journal of Microscopy*, **218**(1), 52–61.

Fouke, K. E., Wegman, M. E., Weber, S. A., Brady, E. B., Roman-Vendrell, C., & Morgan, J. R. (2021). Synuclein regulates synaptic vesicle clustering and docking at a vertebrate synapse. *Frontiers in Cell and Developmental Biology*, **9**, 774650.

Greten-Harrison, B., Polydoro, M., Morimoto-Tomita, M., Diao, L., Williams, A. M., Nie, E. H., Makani, S., Tian, N., Castillo, P. E., Buchman, V. L., & Chandra, S. S. (2010). alphabetagamma-Synuclein triple knockout mice reveal age-dependent neuronal dysfunction. *Proceedings of the National Academy of Sciences of the United States of America*, **107**(45), 19573–19578.

Gurry, T., Ullman, O., Fisher, C. K., Perovic, I., Pochapsky, T., & Stultz, C. M. (2013). The dynamic structure of alpha-synuclein multimers. *Journal of the American Chemical Society*, **135**(10), 3865–3872.

Iyer, A., Roeters, S. J., Schilderink, N., Hommersom, B., Heeren, R. M. A., Woutersen, S., Claessens, M., & Subramaniam, V. (2016). The impact of N-terminal acetylation of α-synuclein on phospholipid membrane binding and fibril structure. *Journal of Biological Chemistry*, **291**(40), 21110–21122.

Kang, L., Moriarty, G. M., Woods, L. A., Ashcroft, A. E., Radford, S. E., & Baum, J. (2012). N-terminal acetylation of alpha-synuclein induces increased transient helical propensity and decreased aggregation rates in the intrinsically disordered monomer. *Protein Science*, **21**(7), 911–917.

Kramer, M. L., & Schulz-Schaeffer, W. J. (2007). Presynaptic alpha-synuclein aggregates, not Lewy bodies, cause neurodegeneration in dementia with Lewy bodies. *Journal of Neuroscience*, **27**(6), 1405–1410.

Logan, T., Bendor, J., Toupin, C., Thorn, K., & Edwards, R. H. (2017). alpha-Synuclein promotes dilation of the exocytotic fusion pore. *Nature Neuroscience*, **20**(5), 681–689.

Maltsev, A. S., Ying, J., & Bax, A. (2012). Impact of N-terminal acetylation of alpha-synuclein on its random coil and lipid binding properties. *Biochemistry*, **51**(25), 5004–5013.

Medeiros, A. T., Bubacco, L., & Morgan, J. R. (2018). Impacts of increased alpha-synuclein on clathrin-mediated endocytosis at synapses: Implications for neurodegenerative diseases. *Neural Regeneration Research*, **13**, 647–648.

Medeiros, A. T., Soll, L. G., Tessari, I., Bubacco, L., & Morgan, J. R. (2017). alpha-synuclein dimers impair vesicle fission during clathrin-mediated synaptic vesicle recycling. *Frontiers in Cellular Neuroscience*, **11**, 388.

Miller, D. W., Hague, S. M., Clarimon, J., Baptista, M., Gwinn-Hardy, K., Cookson, M. R., & Singleton, A. B. (2004). Alpha-synuclein in blood and brain from familial Parkinson disease with SNCA locus triplication. *Neurology*, **62**(10), 1835–1838.

Nemani, V. M., Lu, W., Berge, V., Nakamura, K., Onoa, B., Lee, M. K., Chaudhry, F. A., Nicoll, R. A., & Edwards, R. H. (2010). Increased expression of alpha-synuclein reduces neurotransmitter release by inhibiting synaptic vesicle reclustering after endocytosis. *Neuron*, **65**(1), 66–79.

Nuber, S., Rajsombath, M., Minakaki, G., Winkler, J., Muller, C. P., Ericsson, M., Caldarone, B., Dettmer, U., & Selkoe, D. J. (2018). Abrogating native alpha-synuclein tetramers in mice causes a L-DOPA-responsive motor syndrome closely resembling Parkinson's disease. *Neuron*, **100**(1), 75-90.e5.

Parra-Rivas, L. A., Madhivanan, K., Aulston, B. D., Wang, L., Prakashchand, D. D., Boyer, N. P., Saia-Cereda, V. M., Branes-Guerrero, K., Pizzo, D. P., Bagchi, P., Sundar, V. S., Tang, Y., Das, U., Scott, D. A., Rangamani, P., Ogawa, Y., & Subhojit, R. (2023). Serine-129 phosphorylation of alpha-synuclein is an activity-dependent trigger for physiologic protein-protein interactions and synaptic function. *Neuron*, **111**(24), 4006–4023.e10.

Ramalingam, N., Jin, S. X., Moors, T. E., Fonseca-Ornelas, L., Shimanaka, K., Lei, S., Cam, H. P., Watson, A. H., Brontesi, L., Ding, L., Hacibaloglu, D. Y., Jiang, H., Choi, S. J., Kanter, E., Liu, L., Bartels, T., Nuber, S., Sulzer, D., Mosharov, E. V., Chen, W. V., Li, S., Selkoe, D. J., & Dettmer, U. (2023). Dynamic physiological alpha-synuclein S129 phosphorylation is driven by neuronal activity. *NPJ Parkinson's Disease*, **9**(1), 4.

Roman-Vendrell, C., Medeiros, A. T., Sanderson, J. B., Jiang, H., Bartels, T., & Morgan, J. R. (2021). Effects of excess brain-derived human alpha-synuclein on synaptic vesicle trafficking. *Frontiers in Neuroscience*, **15**, 639414.

Runfola, M., De Simone, A., Vendruscolo, M., Dobson, C. M., & Fusco, G. (2020). The N-terminal acetylation of alpha-synuclein changes the affinity for lipid membranes but not the structural properties of the bound state. *Scientific Reports*, **10**(1), 204.

Sanderson, J. B., De, S., Jiang, H., Rovere, M., Jin, M., Zaccagnini, L., Hays Watson, A., De Boni, L., Lagomarsino, V. N., Young-Pearse, T. L., Liu, X., Pochapsky, T. C., Hyman, B. T., Dickson, D. W., Klenerman, D., Selkoe, D. J., & Bartels, T. (2020). Analysis of alpha-synuclein species enriched from cerebral cortex of humans with sporadic dementia with Lewy bodies. *Brain Communications*, **2**(1), fcaa010.

Schechter, M., Atias, M., Abd Elhadi, S., Davidi, D., Gitler, D., & Sharon, R. (2020). alpha-Synuclein facilitates endocytosis by elevating the steady-state levels of phosphatidylinositol 4,5-bisphosphate. *Journal of Biological Chemistry*, **295**(52), 18076–18090.

Schulz-Schaeffer, W. J. (2010). The synaptic pathology of alpha-synuclein aggregation in dementia with Lewy bodies, Parkinson's disease and Parkinson's disease dementia. *Acta Neuropathologica*, **120**(2), 131–143.

Scott, D., & Roy, S. (2012). α-synuclein inhibits intersynaptic vesicle mobility and maintains recycling-pool homeostasis. *Journal of Neuroscience*, **32**(30), 10129–10135.

Scott, D. A., Tabarean, I., Tang, Y., Cartier, A., Masliah, E., & Roy, S. (2010). A pathologic cascade leading to synaptic dysfunction in alpha-synuclein-induced neurodegeneration. *Journal of Neuroscience*, **30**(24), 8083–8095.

Selkoe, D., Dettmer, U., Luth, E., Kim, N., Newman, A., & Bartels, T. (2014). Defining the native state of alpha-synuclein. *Neurodegenerative Diseases*, **13**(2–3), 114–117.

Sharma, M., & Burre, J. (2023). alpha-synuclein in synaptic function and dysfunction. *Trends in Neuroscience (Tins)*, **46**(2), 153–166.

Singleton, A. B., Farrer, M., Johnson, J., Singleton, A., Hague, S., Kachergus, J., Hulihan, M., Peuralinna, T., Dutra, A., Nussbaum, R., Lincoln, S., Crawley, A., Hanson, M., Maraganore, D., Adler, C., Cookson, M. R., Muenter, M., Baptista, M., Miller, D., … Gwinn-Hardy K. (2003). alpha-Synuclein locus triplication causes Parkinson's disease. *Science*, **302**(5646), 841.

Soll, L. G., Eisen, J. N., Vargas, K. J., Medeiros, A. T., Hammar, K. M., & Morgan, J. R. (2020). alpha-synuclein-112 impairs synaptic vesicle recycling consistent with its enhanced membrane binding properties. *Frontiers in Cell and Developmental Biology*, **8**, 405.

Spillantini, M. G., Crowther, R. A., Jakes, R., Hasegawa, M., & Goedert, M. (1998). alpha-Synuclein in filamentous inclusions of Lewy bodies from Parkinson's disease and dementia with lewy bodies. *Proceedings of the National Academy of Sciences of the United States of America*, **95**(11), 6469–6473.

Spinelli, K. J., Taylor, J. K., Osterberg, V. R., Churchill, M. J., Pollock, E., Moore, C., Meshul, C. K., & Unni, V. K. (2014). Presynaptic alpha-synuclein aggregation in a mouse model of Parkinson's disease. *Journal of Neuroscience*, **34**(6), 2037–2050.

Sulzer, D., & Edwards, R. H. (2019). The physiological role of alpha-synuclein and its relationship to Parkinson's Disease. *Journal of Neurochemistry*, **150**(5), 475–486.

Theillet, F. X., Binolfi, A., Bekei, B., Martorana, A., Rose, H. M., Stuiver, M., Verzini, S., Lorenz, D., van Rossum, M., Goldfarb, D., & Selenko, P. (2016). Structural disorder of monomeric alpha-synuclein persists in mammalian cells. *Nature*, **530**(7588), 45–50.

Vargas, K. J., Makani, S., Davis, T., Westphal, C. H., Castillo, P. E., & Chandra, S. S. (2014). Synucleins regulate the kinetics of synaptic vesicle endocytosis. *Journal of Neuroscience*, **34**(28), 9364–9376.

Wallace, J. N., Crockford, Z. C., Roman-Vendrell, C., Brady, E. B., Hoffmann, C., Vargas, K. J., Potcoava, M., Wegman, M. E., Alford, S. T., Milovanovic, D., & Morgan, J. R. (2024). Excess phosphoserine-129 alpha-synuclein induces synaptic vesicle trafficking and declustering defects at a vertebrate synapse. *Molecular Biology of the Cell*, **35**(1), ar10.

Walsh, R. B., Bloom, O. E., & Morgan, J. R. (2018). Acute manipulations of clathrin-mediated endocytosis at presynaptic nerve terminals. *Methods in Molecular Biology*, **1847**, 65–82.

Wang, C., Zhao, C., Hu, X., Qiang, J., Liu, Z., Gu, J., Zhang, S., Li, D., Zhang, Y., Burré, J., Diao, J., & Liu, C. (2024). *N-acetylation of α-synuclein enhances synaptic vesicle clustering mediated by α-synuclein and lysophosphatidylcholine*. eLife Sciences Publications, Ltd.

Wang, L., Das, U., Scott, D. A., Tang, Y., McLean, P. J., & Roy, S. (2014). alpha-synuclein multimers cluster synaptic vesicles and attenuate recycling. *Current Biology*, **24**(19), 2319–2326.

Westphal, C. H., & Chandra, S. S. (2013). Monomeric synucleins generate membrane curvature. *Journal of Biological Chemistry*, **288**(3), 1829–1840.

Xu, J., Wu, X. S., Sheng, J., Zhang, Z., Yue, H. Y., Sun, L., Sgobio, C., Lin, X., Peng, S., Jin, Y., Gan, L., Cai, H., & Wu, L. G. (2016). alpha-synuclein mutation inhibits endocytosis at mammalian central nerve terminals. *Journal of Neuroscience*, **36**(16), 4408–4414.

Additional information

Data availability statement

The raw data supporting the conclusions of this article will be made available by the authors, without undue reservations.

Competing interests

No competing interests declared.

Author contributions

C.R.V., J.N.W., J.R.M. and T.B. contributed to the conception and design of the study. C.R.V. collected and analysed the E.M. data and created the figures. J.N.W. wrote code and performed some of the electron microscopy analyses. M.C., A.H.W. and T.B. purified the proteins and conducted the biochemical analyses.

All authors participated in the writing and editing of the manuscript and approved the final submission.

Funding

This study was supported by NIH research grants to J.R.M. (NINDS/NIA R01NS078165 and RF1NS078165-12), as well as an NIH MOSAIC award to C.R.V. (NINDS K99 NS126575-01) and a Parkinson's Foundation Postdoctoral Fellowship to C.R.V. (PF-PRF-932 736). This work was also supported by grants to T.B. from the UK Dementia Research Institute (DRI), which receives funding from the UK Medical Research Council, the US National Institute of Neurological Disorders and Stroke grants (U54-NS110435, R01-NS109209, RF1NS133979 and R01-NS078165), the Eisai Pharmaceutical postdoctoral programme and the Chan Zuckerberg Collaborative Pairs Initiative Phase 2.

Acknowledgements

The authors would like to thank Louie Kerr and the MBL Central Microscopy Facility for technical assistance with the electron microscopy.

Keywords

clathrin, endocytosis, endosome, Parkinson's disease

Supporting information

Additional supporting information can be found online in the Supporting Information section at the end of the HTML view of the article. Supporting information files available:

Peer Review History